

Published in final edited form as:

Phys Med Biol. 2015 November 21; 60(22): R323–R361. doi:10.1088/0031-9155/60/22/R323.

Radiotherapy Planning using MRI

Maria A Schmidt and Geoffrey S Payne

Cancer Research UK Cancer Imaging Centre, Royal Marsden Hospital and the Institute of Cancer Research, Downs Road, Sutton, Surrey, SM2 5PT, UK

Abstract

The use of Magnetic Resonance Imaging (MRI) in Radiotherapy (RT) planning is rapidly expanding. We review the wide range of image contrast mechanisms available to MRI and the way they are exploited for RT planning. However a number of challenges are also considered: the requirements that MR images are acquired in the RT treatment position, that they are geometrically accurate, that effects of patient motion during the scan are minimised, that tissue markers are clearly demonstrated, that an estimate of electron density can be obtained. These issues are discussed in detail, prior to the consideration of a number of specific clinical applications. This is followed by a brief discussion on the development of real-time MRI-guided RT.

Keywords

MRI; magnetic resonance imaging; radiotherapy; planning

Introduction

Magnetic Resonance Imaging (MRI) is increasingly being used in Radiotherapy (RT) planning owing to its superior soft-tissue contrast compared with CT. The purpose of this short review is to introduce the features of MRI that make it advantageous for radiotherapy planning, to discuss the challenges that this introduces, and how they are being solved, and to indicate the current status in specific applications. Most of the discussion is in the context of external beam radiotherapy (EBRT), but brachytherapy will also be mentioned.

In principle it would be desirable to be able to replace the CT planning scan entirely with a corresponding MRI planning scan. However although the problem of ensuring geometric accuracy and the requirement for an estimate of electron density for the tissue dose calculations are being addressed (see below) in practice MRI is currently mainly used in combination with a standard CT planning scan.

Contrast Mechanisms in MRI

The advantage of MRI compared with CT scanning for radiotherapy planning is the excellent soft tissue contrast. Figure 1 illustrates the difference between CT and MR images of the prostate; in the CT scan it is hard to identify even the boundaries of the prostate,

whereas in the MR image not only the prostate boundary but also a good deal of the internal structure of peripheral zone and central gland is observed. In many cases one or more of the dominant intraprostatic lesions are seen, which raises the additional possibility of targeting a boost dose to this region (Riches et al., 2014, Kim et al., 2008, Pouliot et al., 2004, Singh et al., 2007). Organs at risk (OARs), such as rectum and bladder, are also generally well delineated, and therefore help identify the regions in which minimised doses are desired in the radiotherapy plan.

Depending on the precise imaging sequence used, contrast in MRI has the capability to reflect a range of properties of tissues, which are described below. While for any particular situation it may be possible to predict which MRI contrast mechanism would be optimal based on knowledge of tissues, in practice the choice is often based on experience rather than calculation.

Processes underlying MR image formation

The principles of MR image formation are described in many text books (Plewes and Kucharczyk, 2012, Haacke et al., 1999, McRobbie et al., 2003). Briefly, MR images are formed from tiny signals induced by atomic magnetic dipoles when they precess coherently in a strong magnetic field. Most clinical MRI systems use superconducting magnets with a field strength of 1.5 or 3 Tesla. In MRI the signals of interest are mainly from ^1H nuclei (spin $\frac{1}{2}$) in water, although signals from ^1H nuclei in other mobile compounds (mainly lipids) will also be detected. MRI signals from other nuclei of biological interest with magnetic dipole moments (e.g. ^{31}P , ^{23}Na , ^{13}C) are intrinsically much smaller than those from ^1H nuclei. They are produced at frequencies well outside the frequency bandwidth of ^1H MRI measurements, and are not routinely used in clinical imaging.

At thermal equilibrium the orientation of the transverse component of the nuclear magnetic dipoles is random, with the net magnetisation parallel to the magnetic field. Radiofrequency (RF) pulses are applied to rotate the magnetisation into the transverse plane; the resulting coherent precession of the magnetic dipoles then induces signals in the MR receiver coils. Pulses of current in magnetic field gradient coils create short-term additional magnetic fields which vary linearly in specified directions (x, y, z) and enable the MRI signals to be localised to create the image.

The individual nuclear spins within the magnetisation vector gradually get out of phase with each other, causing the net magnetisation (and hence the MRI signal) to decay. This decay process is often approximated well as an exponential decay, with the transverse relaxation time constant, T_2 , usually of the order of 30 to 100 ms. There is also a slower relaxation along the direction of the main field, which again can be approximated by the longitudinal relaxation time constant, T_1 , typically of the order of several hundred ms. In general more fluid tissues tend to have longer T_1 and T_2 relaxation time constants, except for paramagnetic effects such as those caused by deoxyhemoglobin, and by administered contrast agents (see below). Water in tissues containing or near to discontinuities of magnetic susceptibility will experience significantly non-uniform magnetic fields which enhances spin dephasing and hence the rate of transverse relaxation; the corresponding

enhanced transverse relaxation time constant which includes this effect is given the symbol T_2^* .

MR Image Contrast Mechanisms

Magnetic resonance images are created using signals produced by the motion of the nuclei of mobile hydrogen atoms in a strong magnetic field, primarily from ^1H in tissue water and fats (lipids). It is possible to acquire MR images which reflect the relative amounts of water in different tissues. For historical reasons these images are known as “proton density” images, since ^1H nuclei are just protons. However proton density images give relatively little contrast between soft tissues and the real power of MRI is in allowing other mechanisms to determine the image contrast. Allowing image intensity to be weighted by the T1 and T2 of the tissues not only permits faster scanning but gives more contrast in the images. **T1-weighted images** show relatively more signal from tissues with a short T1, and are obtained using acquisition sequences with a repetition time (TR) which is short relative to the tissue T1. **T2-weighted images** show relatively higher signals from tissues with a long T₂, and are obtained using acquisition sequences with an echo time (TE) that is of similar duration to the tissue T2. T1w and T2w imaging have been the primary mechanisms for tissue contrast since the first development of MRI. Examples of T1 and T2-weighted images are shown in Figure 2a and 2b.

Contrast agents in MRI are generally paramagnetic, and produce a strong reduction in T1 and/or T2 of nearby hydrogen nuclei. The most commonly used contrast agents are based on a gadolinium chelate, with the dominant effect of reducing T1. Tissues accessed by these gadolinium agents therefore appear bright in a T1-weighted image. In high-grade brain tumours, for example, the blood-brain barrier is sufficiently disrupted to allow gadolinium chelates to leak out of blood vessels into the extracellular space, leading to signal enhancement (Figure 2c). In contrast super-paramagnetic iron oxide particles (SPIOs) lead to signal loss in T2-weighted images. They are used for liver and spleen imaging, where normal Kupffer cells take up the contrast agent and become darker while pathological tissues remain bright (Tanimoto and Kuribayashi, 2006). SPIOs can also be used to test for lymph-node integrity; normal lymph nodes will take up these particles and lose signal, while those parts of lymph nodes containing tumour will remain relatively bright (Koh et al., 2009, Harnan et al., 2011, Jahan et al., 2010).

In **Dynamic Contrast-Enhanced MRI (DCE-MRI)** T1-weighted images are acquired during and for about 4–6 minutes after the administration of the contrast agent (Tofts and Kermode, 1991). Rapid 3d volume coverage is required to give the necessary time resolution of about 10s. The changes in the T1-weighted signals reflect the leakage of the contrast agent from the vasculature into the interstitial space. The relatively leaky immature vasculature of tumours leads to a more rapid uptake and washout compared with that of normal tissues (Fig 3a). Evaluation can be done visually according to curve shape, quantitatively using model-independent parameters such as time to peak enhancement, or quantitatively using a multi-compartment model to obtain estimates for parameters such as K^{trans} (the product of surface-area & permeability), v_e (volume fraction of extracellular space) and v_p (the plasma fraction (Verma et al., 2012, Tofts and Kermode, 1991)). These

results can be calculated on a pixel by pixel basis and presented as an image (Fig 3b). Mechanical injectors are generally used to ensure a uniform and rapid injection. In addition to characterising tissue, DCE-MRI is also used to evaluate response to treatment, in particular antiangiogenic and antivascular therapies (Ferl and Port, 2012).

Perfusion parameters such as blood flow and volume may be estimated using **dynamic susceptibility contrast (DSC) MRI**. The passage of a bolus of gadolinium-based contrast agent through the vasculature leads to a transient large gradient of magnetic field around the blood vessels. The consequent spin dephasing in these regions reduces signal in T2*-weighted images. While spin-echo sequences refocus this dephasing for stationary spins, any diffusion of spins into regions of different magnetic field during the measurement echo time leads to a degree of irreversible dephasing that leads to reduced signal in T2-weighted images. The change in T2-weighted signal is more sensitive to small blood vessels than that of T2*-weighted imaging (Kennan and Jager, 2003). While DSC MRI can be used in any tissue, its main application has been in the brain for measurement of regional cerebral blood volume (rCBV), and regional cerebral blood flow (rCBF) (Calamante, 2010). As with all of the more sophisticated MR imaging methods, care is required in data acquisition and processing in order to achieve good quality results (Willats and Calamante, 2013).

Blood oxygenation level dependent (BOLD) imaging is based on the same principles as DSC but instead of using administered contrast agents it takes advantage of the difference in magnetic susceptibility between oxyhemoglobin (diamagnetic) and deoxyhaemoglobin (paramagnetic) to provide the change in spin dephasing around blood vessels (Huettel et al., 2009). The main application of this technique is in so-called functional MRI (fMRI) for detecting brain activation during specified cognitive tasks, such as finger tapping, visual stimulation, and memory tasks. These tasks stimulate increased blood flow to the relevant region in the brain with a corresponding change in signal intensity. These changes are small but significant, and have been useful in identifying which parts of the brain are involved in different brain activities. Signal changes are very small, so careful statistical methods are required to correctly identify the region of activity (Ashby, 2011). In the context of radiotherapy planning, such measurements are helpful in designing treatment plans to avoid critical structures.

MRI signals can be made sensitive to diffusion processes in tissue by inserting paired pulses of magnetic field gradient in spin-echo sequences. The principle was first proposed by Stejskal and Tanner in 1965 (Stejskal and Tanner, 1965), and has subsequently been incorporated into MR imaging sequences. Tissues with relatively unrestricted diffusion will lose signal and appear dark on a **diffusion-weighted image** (e.g. in body fluids, CSF etc), while tissues characterised by restricted diffusion will appear brighter. Often a series of images is acquired with increasing diffusion-weighting, from which the **“apparent diffusion co-efficient” (ADC)** may be calculated for each pixel and represented as an ADC image. These have the reverse contrast to the diffusion-weighted images, so that areas of high (un-restricted) diffusion now appear brighter. In many tissues the diffusion-weighted signal appears to be dominated by the extracellular water, so that tissues with a smaller proportion of extracellular space (often denoted as having “high cellularity”) have more restricted diffusion and appear darker. Note that the apparent diffusion co-efficient is usually

dominated by the barriers to molecular diffusion such as cell membranes and organelles, and therefore reflects the restricted diffusion of the molecules studied (usually tissue water) rather than the intrinsic diffusivity of the unrestricted medium.

In many tissues, diffusion processes are not isotropic. For example in the brain the diffusion is more restricted across the myelin fibres than parallel to them. Diffusion processes can be mapped as a function of direction using **Diffusion Tensor Imaging (DTI)** and then related to internal tissue structure. The main application of DTI is in studying connectivity of fibres in the brain (Jones, 2011), which can be helpful in planning treatment to the brain. This technique is often referred to as diffusion tractography.

The appearance of tumours in diffusion-weighted images will depend to some extent on the nature of the surrounding tissue. In normal prostate for example the tissue is characterised by a large number of prostatic ducts with a corresponding relatively unrestricted diffusion; tumours with a higher cell density therefore appear brighter on a diffusion-weighted image, and darker on an ADC map (see Figure 4), with the degree of ADC reduction correlating with increasing Gleason grade of the tumour (Hambrock et al., 2011). ADC is also reduced in breast tumours (Rahbar et al., 2013) while in brain it depends on the nature of the lesion whether the ADC is higher or lower than surrounding brain (Peet et al., 2012). In the brain the reduction in anisotropy correlates with tumor cellularity and percentage tumor infiltration (Stadlbauer et al., 2006). However in other tissues (except kidney and muscle) anisotropy effects are small and isotropic measures of ADC tend to be used (Padhani et al., 2009).

MRI can also use additional applied gradients to produce images sensitive to coherent motion, such as the motion of blood within blood vessels. This technique, known as **MR Angiography (MRA)**, can be made sensitive to the direction of flow, and can map arterial and venous blood supply separately. A similar result can be achieved by making use of contrast-agents in contrast-enhanced MRA (Hartung et al., 2011). Although MRA has not been widely used in RT planning, it has been used in radiosurgery for evaluating arterial-venous malformations (Buis et al., 2007) and has potential value in targeting lymph nodes and other structures located along vessel pathways.

Magnetic resonance spectroscopy uses the same principles and equipment as MRI, but is designed to detect signals from compounds other than water in tissues. These compounds include low molecular weight metabolites such as creatine, choline, some amino acids, and lactate, and fats (which have high concentration in adipose tissues but are also present to smaller extents elsewhere). MR spectra are usually acquired either from a single target voxel or from a 2d or 3d grid of voxels (Figure 5). This latter method is called magnetic resonance spectroscopic imaging (MRSI). Methods of acquisition and processing of MR spectra are well-described by de Graaf (2007).

The different biochemical composition of tissues detected using MRS can be used for differential diagnosis (Howe et al., 2003). Many cancers are characterised by high levels of choline relative to normal tissues, while some compounds normally found in tissue (such as N-acetyl aspartate in brain, and citrate in prostate) are reduced (Glunde et al., 2011b).

Amongst other observations, it has been found that the region of metabolic abnormality in tissue is often different to the region of morphological abnormality seen by regular MR imaging, and is sometimes larger (Nelson et al., 2002).

Signals from other magnetic nuclei (e.g. ^{31}P , ^{13}C , ^{19}F , ^{23}Na) are also probed using magnetic resonance spectroscopy. These require radiofrequency hardware designed to operate at the appropriate frequency and tend to produce smaller signals than ^1H nuclei. In oncology ^{31}P MRS is most used to monitor tumour response to therapy, especially in the new era of targeted treatments that are designed to block specific signalling pathways (Glunde et al., 2011a). Pretreatment ^{31}P MR spectra have also been shown potential to predict final tumour response (Arias-Mendoza et al., 2013). ^{13}C nuclei have only 1% natural abundance, as well as intrinsically only yielding 1.6% of the signal of ^1H nuclei. However the recently developed technique of dynamic nuclear polarisation enables samples to be pre-polarised by factors of approximately 10,000 (Ardenkjaer-Larsen et al., 2003). The initial translation of this methodology to application in human subjects has recently been achieved, with the first clinical trials using the method to detect and evaluate tumours just starting (Nelson et al., 2013).

Positron emission tomography can also be used to probe aspects of tissue metabolism. It requires radio-labelling of exogenous agents, such as fluoro-deoxyglucose, but can detect signals at much lower concentrations (10^{-12} molar) than MRS (mM) and therefore yields complementary information. Recently combined MR-PET systems have become available in which MR and PET data are acquired within the same examination (Partovi et al., 2014, Gaertner et al., 2013). This has required huge technological hurdles to be overcome to avoid serious image degradation in both modalities. The more straightforward approach is the tandem system of Philips, in which the patient on a single bed is first inserted into an MR scanner and then into a PET scanner (Vargas et al., 2013). The simultaneous approach of the Siemens mMR Biograph system (Delso et al., 2011) is clearly much more demanding technologically but is more efficient and permits the following of dynamic processes using both MRI and PET simultaneously. For radiotherapy planning this gives the opportunity to obtain the complementary functional imaging information provided by PET and MRI in a single examination.

Additional Advantages of MRI for Radiotherapy Planning

MRI uses low amplitude non-ionising radio waves, unlike CT scanning which uses ionising radiation. MRI is of particular benefit for paediatric populations in which radiation dose needs to be carefully controlled, and in cases where repeat scans are helpful during treatment both to ensure that the treatment plan is revised to follow radiation-induced tissue changes, and also to monitor early response.

Another feature of MRI is that owing to the method of data acquisition the slice orientation is not required to be transaxial, as it is for CT, but can be sagittal, coronal, or at any oblique angle desired. This enable images to be better aligned with anatomy. However most radiotherapy planning software still assumes that images are acquired in the transverse plane, and it may be a while before this particular feature of MRI can be optimally utilised.

Tumours in many tissues experience movement not just between treatment fractions, but also during fractions. While breath-holding (and active breathing control) is one approach, there is some residual variation between tumour position between sub-fractions. Another potential approach is to adjust the treatment during the fraction dynamically. Radiation dose and poor soft-tissue contrast exclude CT scanning for this purpose, but both ultrasound and MRI have potential for real-time RT guidance. Real-time MR-guided RT is now under development and clinical trial. The current status of this technology was reviewed by Lagendijk et al (2014). MRI has been integrated with LINACs and Cobalt units in different approaches. As with the MR-PET combination, it has been a huge challenge to combine the modalities together, so that both the imaging and the treatment behave as required, in particular to operate the accelerator close to the magnetic field, and to gain access for the beam into the centre of the magnet, and to avoid significant RF interference from the accelerator into the images. While not yet widely available, these developments hold great promise.

The Challenges of using MRI for Radiotherapy Planning

MR images are primarily used to outline the tumour volume and organs at risk, but can also provide information on the excursion of relatively mobile organs and tissues in the presence of physiological motion. Therefore the MRI examination is ideally undertaken with the patient in the RT treatment position. Unlike CT, MRI does not provide a direct measurement of electron density. Although the latter can be estimated from MR images it is most common to perform both MRI and CT examinations in the treatment position and to fuse both datasets after registration. The combined CT-MR dataset contains both the information required for targeting (MRI-based volumes) and for dose calculations (CT-based electron density).

MRI in RT Treatment Position

The typical duration of the image acquisition process in MRI is of the order of minutes, while CT is often undertaken in seconds – a timescale more directly comparable to that of RT fraction delivery. Most diagnostic MRI examinations include the acquisition of several series of images with different contrast characteristics. MRI beds with soft padding, sometimes concave, ensure patient comfort over the typical duration of an MRI examination, but are not necessarily compatible with RT positions. Unfortunately, adapting MRI examinations to the RT treatment position may involve a degree of compromise in image quality.

For many years the standard 60 cm internal diameter MRI system was the widest superconducting horizontal magnet available, limiting the range of RT treatment positions that could be reproduced during the MRI examination. The alternative for patient positions requiring additional width was an open magnet, which imposes fewer restrictions on patient position. However, open magnets are characterised by lower magnetic fields (typically 0.5 T), and therefore are not expected to reach the same signal-to-noise ratio (SNR) as the 1.5 T systems commonly available. In addition the open bore also restricts the design of the gradient coils and open MR systems are more likely to be affected by geometric distortion. Currently 70 cm bore systems are becoming widely available at 1.5 T and 3.0 T; it is now

possible to raise the patients' arms above their head within the magnet and to use wing boards. The only common treatment position not feasible within a 70 cm system is the breast position with the elbows outstretched at shoulder level.

All the main manufacturers of MRI equipment have responded to the demands of the radiotherapy users and now provide auxiliary equipment to enable most examinations to take place in the treatment position. Rigid flat beds are available to be placed over the standard MRI couch, and additional receiver coil configurations are possible for situations where the patient position prevents the use of standard receiver coil arrangements. Most patient positioning devices have MR-compatible versions available, avoiding ferromagnetic components and conductive materials (e.g. carbon fibre). Examples are head and neck examinations making use of a flat bed, head board and thermoplastic mask, but which cannot take place within the dedicated head and neck receiver coils provided by all MRI manufacturers. It is also possible to employ devices to raise existing receiver coils above the abdomen and thorax, thus preventing the coil weight from disturbing patient anatomy¹. Many other devices and configurations are possible, and many are home-built by users within the MRI and RT communities (Figure 6).

The drive towards reproducing the RT treatment position within the MRI environment can compromise MR image quality. MRI RF receiver coils are affected by the conductivity of the subject and they work optimally under the conditions they were designed for. Spine elements of a phased-array receiver coil are often embedded in the patient couch; the flat bed introduces a gap between coil and patient which reduces signal-to-noise ratio (SNR) performance. The same process occurs when a body surface RF coil array is lifted away from the patient. A head and neck examination undertaken with general purpose RF surface coils is unlikely to reach the same quality as the examinations undertaken with the dedicated head and neck receiver coils, designed to place all elements as closely to the volume of interest as possible. This clear compromise suggests that RT positioning equipment should be used with care, always ensuring that the MR examination reaches sufficient image quality. It is often necessary to adapt MRI protocols to the receiver coil arrangement used for RT planning, and in some cases the data acquisition may need to be longer to compensate for SNR reduction.

MRI scanners have lasers embedded at the front of the magnet bore. These are used to identify a region of interest on the patient which is then translated to the magnet isocentre for optimal imaging. These lasers are often inadequate for RT purposes, and their location does not allow staff to adjust the patient position easily. For best access to the patient RT lasers are mounted outside the MRI bore, either on the walls of the magnet room or as a self-standing structure². In either case the fitting of lasers is best planned ahead of the MRI installation. Fitting lasers retrospectively to an operational MRI system imposes a prohibitive risk to the integrity of the Faraday cage.

¹<http://www.healthcare.siemens.com/magnetic-resonance-imaging/mri-guided-therapy/magnetom-combi-suite/use>

²<http://www.lap-laser.com/>

Geometric Accuracy of MR Images

MRI makes use of magnetic field gradients to provide a linear relationship between resonant frequency and position, and hence to assign signals to their spatial origins. As a consequence, imperfections in the static magnetic field uniformity and gradient linearity may lead to geometric distortion of MR images. In addition, the patients themselves disturb the magnetic field with their own particular spatial distribution of magnetic susceptibilities, causing a degree of patient-dependent image distortion. Both system-related and patient-related causes of geometric distortion are undesirable for RT planning, and must be quantified and minimised.

System-Related Geometric Distortion—In ideal conditions MR images are generated by superimposing a constant and linear magnetic field gradient to a uniform static magnetic field. In practice there are design constraints on magnet size and conflicting demands for gradients of high magnitude and high slew rates. The final compromise often leads to geometrical image distortions which increase away from the magnet isocentre, reaching a few centimeters at the edges of the scanner's maximum field of view (Doran et al., 2005, Wang and Doddrell, 2005). In addition to the geometric distortion in the readout and phase encoding directions, the selective RF excitation is also affected, causing warping of the excited slice (or slab) and thickness changes as a function of position. The use of high imaging gradient amplitudes makes the sequences less sensitive to the non-uniformity of the static magnetic field, but this requires an increase in bandwidth. Higher receiver bandwidth leads to reduction in SNR and higher excitation bandwidth requires more radiofrequency power to be applied to the patient. In addition, higher imaging gradients may lead to distortion of gradient waveforms, which in turn may cause further geometric distortion. Therefore a careful choice of pulse sequence parameters is required for applications which rely on geometric integrity: radiotherapy planning, stereotactic surgery (Tavares et al., 2014) and accurate geometric measurements (Jovicich et al., 2006).

Baldwin et al. (2007) characterised geometric distortion for different sequences, and demonstrated that gradient non-uniformity is the main source of distortion in basic anatomic pulse sequences. The gradient non-uniformity is expected to be stable and independent of the pulse sequence applied. Ahmed et al. (2010) and Mizowaki et al. (2000) made many measurements of geometric distortion over periods of seventeen months and six months, respectively; both articles report temporal stability. However, a degree of caution is appropriate: sequences involving fast gradient switching are also affected by eddy-currents which may distort gradient waveforms. The geometric distortion associated with faster sequences could be less stable, and further information is required to ascertain their reliability.

Distortion correction for gradient imperfection can be performed on 2D images or 3D volumes. Because the distortion in itself affects all directions, the use of 3D correction on a 3D volume is likely to be more successful. However, post-processing for correction of geometric distortion can degrade image quality and change noise characteristics as the acquired voxels of the original images are either contracted or extended.

The main MRI vendors have incorporated post-processing for distortion correction to their products, and this can be applied automatically with minimal increase in image reconstruction time. Once the system-based geometric distortion is known, it can be corrected by using a transformation from the real coordinate system to an undistorted one, a process akin to non-rigid image registration. The function describing this transformation is either a global mathematical description of the distortion or a localised one. Spherical harmonics (Janke et al., 2004), polynomials (Maikusa et al., 2013), splines (Caramanos et al., 2010) and tri-linear interpolations (Wang et al., 2004a) have been used successfully. Using standard vendor's distortion correction, the displacement is greatly reduced, only reaching to 2-3 millimetres on the outer edges of the clinically useful volume (Wang et al., 2004b).

The system-based geometric distortion must be assessed to characterise any MR system providing images for RT planning purposes. Several large three-dimensional structured test objects are described in the literature for that purpose (Doran et al., 2005, Wang et al., 2004a, Caramanos et al., 2010). Imperfections in the manufacture of test objects are overcome by using a CT image, presumed geometrically accurate, as a reference for distortion measurements. The ideal test object should cause minimal disturbance to the static magnetic field due to its own susceptibility. The linear arrangement of long fluid-filled cylindrical tubes presented by Doran et al. (2005) has those characteristics and also has the advantage of being very low weight for the large volume encompassed (Figure 7). The hypothesis that the distortion introduced by the test object's own susceptibility is negligible for the sequence tested can (and must) be verified. This can be achieved either by comparing images acquired with different receiver bandwidth or images acquired with readout gradients in opposite directions (Chang and Fitzpatrick, 1992).

Patient-Related Geometric Distortion—Patients are primarily diamagnetic due to their high water content, but also contain air spaces and various paramagnetic ions in position-dependent concentrations. The patient's distribution of magnetic susceptibility values disturbs the static field locally, and this disturbance can be very severe in the vicinity of implants and irregularly shaped structures associated with discontinuities in magnetic susceptibility, and hence lead to distortion in MR images. This distortion is characterised by areas of signal loss due to dephasing of MR signals in the presence of field inhomogeneity, and by bright areas associated with the displacement of signals. The later effect is known as signal pile-up (Callaghan, 1991). In addition, differences in the electron density distribution of ^1H atoms in water and fats lead to different degrees of shielding from the applied magnetic field, causing ^1H nuclei in water and fat to produce signals at slightly different frequencies. This phenomenon, named chemical shift, is responsible for the relative displacement of signals originating from water and fat along the readout gradient direction (McRobbie et al., 2003).

MR techniques vary in their sensitivity to magnetic field inhomogeneity and chemical shift. Techniques based on gradient-echoes are most susceptible, particularly if the echo-time is long or if the technique is based on echo trains. **Echo-planar imaging (EPI)**, a very fast imaging technique capable of single-shot acquisitions, is widely used in neurological applications, but is known to produce distorted images in the vicinity of air spaces (Jezzard,

2012). Although the use of parallel imaging can mitigate this effect by shortening echo trains (McRobbie et al., 2003), the direct application of uncorrected EPI-based functional imaging techniques such as DWI, DTI and fMRI to RT planning is very limited.

The approaches described in the previous section to mitigate the effects of inhomogeneity of the static magnetic field also apply to susceptibility-related field inhomogeneity: the use of high readout gradients reduces artifactual displacements either due to magnetic field inhomogeneity or chemical shift, but at the price of increasing levels of noise in the images. The use of high slice selection gradient amplitudes and high excitation bandwidth has a similar effect in maintaining the geometry of the excitation volume, also reducing slice “warping” in multi-slice acquisitions (Reinsberg et al., 2005). In basic anatomical imaging careful bandwidth choice is usually sufficient to ensure adequate overall geometric integrity, even if some localised small scale distortion remains. If distortion from chemical shift effects is a significant factor, fat suppression (or water suppression) can also be employed to produce geometrically accurate images of the remaining signals.

In addition to these approaches it is also possible to improve the geometric integrity of MR images by post-processing, provided that further information is available. The main approaches are (i) mapping of the magnetic field inhomogeneity to correct, for example, EPI-based imaging (Cusack et al., 2003), (ii) model-based non-rigid registration with a reference image, presumed geometrically accurate (Andersson and Skare, 2002), and (iii) combining two datasets acquired with opposite readout gradient polarity (forward and reverse) as suggested by Chang and Fitzpatrick (1992). These techniques show promise, as they can potentially generate geometrically accurate EPI-based functional MRI images, but require validation prior to being brought into wide use in RT planning.

Metal Artifacts and their Reduction—Many metallic implants are MR-safe, but cause severe local artifacts in MR images due to susceptibility-related magnetic field inhomogeneity and to currents induced in the implant by radiofrequency fields and by the imaging gradient fields. Common artifacts are areas of signal loss, bright areas of signal accumulation and local distortions. Previously described strategies can be used to reduce distortion in conventional techniques: the choice of spin-echoes over gradient-echoes, the use of short echo-times (TE) and imaging with high receiver and excitation bandwidth. However, the field inhomogeneity associated with common orthopaedic implants has been shown to be orders of magnitude higher than the naturally occurring field inhomogeneity in biological material (Hargreaves et al., 2011). As a result conventional MRI techniques cannot eliminate completely the artifacts associated with metallic implants. This is a particular challenge for RT planning as CT images also suffer from streak artifacts in the presence of metallic implants. In extreme cases MR-CT registration can be compromised.

Figure 8 shows standard MR and CT images used in prostate bed RT planning for a patient with a double hip replacement. Both CT and MR images are degraded by artifacts and the volume of the MR examination must be extended in the head/foot direction, above and below the hip replacement, to ensure correct registration.

MR manufacturers have responded to this problem by offering specialist MR techniques to minimise the signal loss. This is achieved in part by high imaging gradients, as previously described. In addition, through plane and in-plane distortions are compensated for with further encoding (Koch et al., 2009, Lu et al., 2009, Koch et al., 2011). The resulting images do minimise signal loss, but often at a cost of increasing the total acquisition time. In some cases, specialist techniques introduce some image blurring (Butts et al., 2005). These techniques require validation prior to further use in RT planning but merit further investigation, as they can provide a more reliable MR-CT fusion in the vicinity of metallic implants.

Estimation of electron density

Image intensity in MRI is not directly related to electron density, and this limits the use of MRI-only RT planning and MRI-simulators. MRI can, however, provide an estimate of electron density for RT planning and for accurate PET image reconstruction in PET-MR systems (Martinez-Moller and Nekolla, 2012).

One approach to generating an MRI-based electron density is to employ a CT Atlas and non-rigid registration to transfer the CT information to the patient's 3D MR data set (Uh et al., 2014, Burgos et al., 2013). This approach is most common using a specialist MRI technique employing ultra-short echo times (UTE), typically under 0.5ms; this enables the visualisation of bone, which has a very short $T2^*$ (Robson et al., 2003, Johansson et al., 2011). Atlas approaches rely on a large number of CT-MR pairs and corrections for image intensity variations in MRI (Burgos et al., 2013). The performance of atlas-based approaches was shown to depend on the number of cases included in the atlas when used for RT planning of common head tumours (Uh et al., 2014). Although atlas-based methods have been validated in PET reconstruction, their general use in RT planning is not yet widespread.

MRI datasets can also be segmented to produce an electron density estimate. Although the most basic segmentation is simply to partition the volume of interest into "air" and "tissue" components, assigned to different Hounsfield Units (HU), it has been shown that the correct segmentation of bone is also necessary (Lambert et al., 2011). Bone can be detected by comparing UTE images with conventional MR images, or by segmenting high resolution anatomical images. The electron density of bone has been assigned to a single value (Karloki et al., 2011), to values based on UTE images (Johansson et al., 2011), and to values based on the $T1/T2^*$ ratio (Kapanen and Tenhunen, 2013), all leading to fairly small deviations from the standard dose calculation. Jonsson et al. (2013) used bulk electron density assignments for different tissue types at various sites (prostate, lung, head and neck, brain), and found that the dose calculation accuracy is not significantly compromised when using MRI data. In addition, fat-based and water-based tissue components can be separated using Dixon techniques which utilise the chemical shift differences between water and fat (McRobbie et al., 2003).

Methods to estimate MR-based electron density are evaluated by considering the deviations in the MRI-based dose distribution, considering the CT-based electron density as a gold standard. General evaluation of MR-based electron density maps are encouraging, but need to be expanded to larger numbers of subjects prior to being placed in general use (Korsholm

et al., 2014, Karotki et al., 2011, Lee et al., 2003). Lambert et al. (2011) demonstrated errors associated with differences in patient external contours introduced by the MR couch top and receiver coil. Johansson et al. (2014) have used different fast MRI techniques based on parallel imaging to assess how quickly a suitable MRI data set can be acquired for head RT planning and how data truncation affects the resulting estimated electron density; his results suggest that many gains in shortening data acquisition time are offset by increased image reconstruction times, making sparse reconstructions less effective in clinical situations.

Motion

In MRI the signal-to-noise ratio is proportional to the voxel size and to the square root of the number of averaged measurements. High spatial resolution therefore requires long data acquisitions; a high-resolution 3D dataset may take up to 10 minutes of data acquisition if a large volume is to be covered with sufficient image quality (a whole pelvis, for example, allowing outlining of tumour, organs at risk, vessels and lymph nodes). This approach is not suitable for volumes affected by physiological motion; apart from blurring, motion in MRI causes ghosts which reproduce the moving structure periodically along the phase-encoding direction, obscuring stationary parts of the volume (Wood and Henkelman, 1985). A number of gating techniques is available in MRI to produce diagnostic images in the presence of cardiac and respiratory motion. However a crucial point is that the volume outlined in MRI must relate to the tumour volume as positioned during RT delivery.

RT can be delivered during breath-holds, can be gated with respiration and can be delivered during free breathing. In addition, a number of devices can be used to restrict the range of motion associated with respiration, based on elastic materials which distribute pressure over the abdomen and pressure pads directly applied to the anterior surface of the abdomen³. These devices are not necessarily MR-compatible, and may need to be adapted to the MRI environment and evaluated over the longer timescale of MRI examinations. Respiratory motion is only approximately periodic and causes significant artifacts in abdominal MRI. Physiological motion may not be significant during RT, but significant during the MRI examination, often substantially longer. It is not necessarily possible to match the breathing status during RT fraction delivery and during MRI examination.

If RT is delivered during free-breathing, MRI is often employed to assess the range of tumour motion (Brix et al., 2014, Marx et al., 2014, Blackall et al., 2006) and to inform on the margins added to the CTV. The implicit compromise between time and spatial resolution suggests that the fast MRI techniques used to follow motion in 3D may not provide sufficient detail for outlining the CTV. As a result, motion assessment and CTV outlining may be done separately. It has been shown that end-expiration breath-holds are most similar to the time averaged images acquired during free breathing, as more time is spent at end expiration during a normal breathing cycle (Seppenwoolde et al., 2002). Thus end-expiration breath-hold MRI may be preferred for registration with CT.

³CIVCO body lok pressure pad.
<http://www.civco.com/ro/products/Stereotactic-Body-Radiation-Therapy-SBRT.htm>

RT can be delivered during breath-holding, using consecutive breath-holds to deliver a given fraction. However consecutive breath-holds are known not to reproduce the same lung volume, and therefore the registration of MRI and CT images may not be adequate even if both were acquired during breath-holding. To minimise the variability in tumour position, RT can make use of breathing-control devices which maintain the same level of lung inflation in consecutive breath-holds⁴. These devices are not necessarily MR-compatible and need to be adapted and evaluated in the MRI environment (Kaza et al., 2015).

RT delivery can also be gated according to the respiratory motion. Devices to monitor respiratory motion are based on bands around the waist, optical tracking devices placed over the chest wall, and devices to control the volume of air taken in inspiration. To be useful, the same device to be used to gate RT delivery must be used during imaging, and with the same gating arrangement. This approach can potentially lead to good registration between MRI and CT, acquired under the same conditions as the RT delivery. Further development in this field is hindered by the longer timescale of the MRI acquisitions.

Jagsi et al. (2007) measured displacement of cardiac structures (particularly the left anterior descending artery) in shallow breathing, breath-holding and breath-holding with active breathing control, and found complex interactions between respiratory and cardiac motion, which are particularly relevant for breast and lung RT. As a result, different approaches are possible for the delivery of RT in the vicinity of the heart (Topolnjak et al., 2012, Wang et al., 2012b). For lower abdominal examinations other complex interactions are expected between respiration and digestive processes, rectal and bladder filling. Figure 9 illustrates that CT-MR fusion can be difficult even when using a flat-bed for the MRI examination: bone landmarks coincide while soft tissues have been considerably displaced. This put emphasis on the standardisation of patient preparation and the development of local procedures for each examination. The use of abdominal and pelvic MRI for several RT applications is discussed in the following section.

Tissue Markers—The motion of many structures is complex and cannot easily be controlled. Examples are prostate motion, associated with rectal and bladder filling, and the motion of some oesophageal tumours, affected by cardiac motion, respiratory motion and digestion. For highly mobile structures it is desirable to implant metallic markers in the vicinity of the tumour, or tumour bed, to enable co-registration of MR and CT images and in some cases dynamic tracking of the target volume during robotic RT delivery (Calcerrada Diaz-Santos et al., 2008). Markers are not usually implanted in the tumour itself, but into the surrounding tissues. A set of three non-co-linear markers centred on a tumour is the minimum requirement to locate the lesion in 3D. It is common to have two collinear markers, and a separate insertion for further markers, to minimise the disruption of tissue adjacent to the lesion. In practice there are constraints and the position of the markers in relation to the lesions is sometimes sub-optimal.

⁴ElekTa Active Breathing coordinator

http://www.elekta.com/healthcare-professionals/products/elekta-oncology/treatment-techniques/motion-management/active-breathing-coordinator.html?utm_source=active-breathing-coordinator&utm_medium=redirect&utm_campaign=redirects

Markers used in MRI need to be MR-compatible and visible in both MR and CT examinations. Most markers are based on inert metals (gold and titanium, for example). Gold seeds employed in prostate RT are approximately 1mm in diameter, but larger cylindrical markers are also available. In either case, the marker itself provides no MR signal and is seen as a signal void, surrounded by visible tissues. It is also possible to emphasise the marker visibility by ensuring that significant signal loss is associated with the differences in susceptibility between the marker and the surrounding tissue. This is done by selecting sequences which enhance T2*-related signal loss (Jonsson et al., 2012, Seevinck et al., 2011). It is also possible to detect off-resonance signals in the vicinity of a marker, which provide positive contrast for the markers (Vonken et al., 2013, Dong et al., 2014), and to map directly susceptibility and susceptibility gradients in the vicinity of the marker (Varma et al., 2011). Clinical studies suggest very good registration between MRI and CT, with only a few millimetres discrepancy between markers centroid (Kapanen et al., 2013, Jonsson et al., 2012). However marker migration and deformations between fractions are also observed (Nichol et al., 2007).

Although there are different approaches to visualising the markers with different MRI pulse sequences, the best marker images will not necessarily have the best contrast for effective visualisation of the tumour and organs at risk. It is often necessary to combine two separate sets of MR images, one with contrast optimised for visualisation of the markers and other with contrast optimised for visualisation of the tumour.

In addition to implanted markers, gel-based surface markers visible in CT, MR and PET images are available to aid the registration of datasets acquired in the same position (Figure 10). Many of those markers are MR compatible but despite that they may still cause a localised decrease in field homogeneity. Their use must be assessed on a case-by-case basis, particularly in cases where EPI-based functional imaging techniques are used.

Limitations of RT and MRI workstations

Radiotherapy planning systems are designed to display imaging data in 2D and 3D and to allow users to delineate 3D volumes (tumours, organs at risk) to which margins are later added, prior to treatment planning. However RT systems were originally designed for CT datasets, which are invariably transaxial. RT planning systems vary in their ability to handle MRI DICOM data; currently some handle transaxial images only, some accept either transaxial, sagittal or coronal images and fewer still handle MRI datasets acquired in oblique orientations. This can be a problem for MRI examinations, as diagnostic MRI examinations are most likely to be orientated around anatomical landmarks, and MRI-trained personnel generally make use of MRI's flexibility in choosing orientation of the volume of interest. This makes it necessary to know the restrictions of a given planning system prior to MRI data acquisition, and therefore limits the overlap of MRI examinations done for diagnostic and planning purposes. In addition RT planning systems do not necessarily handle multiple MRI series with different contrast, and do not always allow flexible transfer of image registration parameters between different series.

MRI workstations do not in general support RT DICOM structures, such as 3D regions of interest, making it more difficult to transfer information between RT systems and MR

workstations. This is particularly relevant when functional MRI is used, as RT systems are not usually equipped to handle image series containing more than one image per location. Examples of the latter are series of DW images containing images of the same slice with different diffusion sensitisation coefficient values (b-values), and DCE image series, containing images of the same slice at different time points. In general not all functional MRI techniques have DICOM support; some pharmacokinetic modelling is undertaken off-line with in-house software which reports in private formats.

As MRI becomes more widely used in RT planning, treatment planning software is expected to evolve to enable routine integration of MRI, enabling the use of all of its features. In addition, MRI workstations are also expected to incorporate RT-friendly features to enable MRI Radiologists and Physicists to contribute further information towards RT planning, including regions of interest.

Applications, Current Status and Future Perspectives

Brain, Head & Neck, and Spine

The use of MRI in neurology is standard practice and the introduction of MRI for planning of radiotherapy and stereotactic surgery of brain lesions has a long history (Flickinger et al., 1992, Khoo et al., 1997) and is widespread (Creak et al., 2011). It is possible to acquire good quality 3D high-resolution MR images (typically 1 mm isotropic resolution), either T1-weighted or T2-weighted, within 5 to 10 minutes. T1-weighted images acquired after administration of contrast agents are used for identifying enhancing lesions and T2-weighted images (with or without fluid attenuation) are used for non-enhancing lesions (low grade gliomas, for example (Stall et al., 2010)). For intra-cranial tumours, the standard MRI head coil is used and a different head position is acceptable, as the RT target is within the rigid structure of the skull. Care must be taken if the lesion is in the brainstem and base of skull, where neck position may affect the position of the target and OAR. For imaging head-and-neck tumours, it is preferred to undertake MRI in the radiotherapy planning position, with appropriate immobilisation devices (such as a thermoplastic mask). This position is incompatible with the standard MR head coil and this examination will require the use of surface RF detection coils (Ahmed et al., 2010). MR protocols must be optimised for this receiver coil configuration, characterised by lower signal-to-noise ratio and less flexibility in using parallel imaging.

The registration of MR and CT datasets is uncontroversial, but a multi-centre trial employing a single head CT-MR test dataset reported an uncertainty of 2 mm in the registration coordinates, with manual registration performing better than automated registration (Ulin et al., 2010). A confounding factor in the registration is the distortion of anatomical MR images due to the patient's own distribution of magnetic susceptibilities. This was quantified by Wang et al. (2013) for brain images; displacements were found to be mostly under 1 mm, but were exceptionally up to 4 mm. Automated and semi-automated segmentation of the clinical target volume is possible (Aslian et al., 2013) and can potentially reduce variability in outlining procedures. Advanced segmentation techniques can use model-based approaches to automate the CTV outlining using a combination of MR images of different

contrast (Nuyts, 2007, Jiang et al., 2013). These techniques are not routinely used, but show promise and are still to be evaluated on large cohorts.

In general the CTV drawn in MR-only images tends to be larger than the one drawn from CT-only images (Ahmed et al., 2010, Fiorentino et al., 2013), but these may simply reflect MRI's sensitivity to oedema, and not necessarily represent a more accurate clinical target volume. A number of studies have attempted to determine the impact of the introduction of MRI to the clinical outcome, by following patient populations after radiotherapy and considering the sites of disease re-occurrence, in relation to the planning volume and dose distributions (for example, Pu et al. (1995)). These studies provide a wealth of information, which is specific to tumour types, tumour sites and radiotherapy technique. A separate issue is the timing of the planning MR examination in relation to other interventions such as surgery and chemotherapy, since both the lesion and the landmarks used for locating it may change (Farace et al., 2011, Minniti et al., 2010, Pirzkall et al., 2009).

In brain lesions, BOLD fMRI has been employed to identify and therefore to spare eloquent areas (Kincses et al., 2012). Diffusion tractography has also been used to spare fiber tracts and functional areas in radiosurgery (Pantelis et al., 2010). Results suggest these functional techniques have a significant impact. Koga et al. (2012) found that the introduction of tractography contributed towards preventing morbidity of radiosurgery in patients with brain arterio-venous malformations. Kovacs et al. (2011) found it possible to reduce the dose to critical organs without compromising dose to the CTV. Large scale studies are therefore required to assess the benefit of these techniques on larger cohorts of patients.

Anatomical T1 and T2 weighted MR images have been employed in Head and Neck cancers, with patients scanned in the treatment position (Bhide et al., 2008, Newbold et al., 2006, Ahmed et al., 2010). Functional imaging was introduced more recently (Quon and Brizel, 2012). DWI (Vandecaveye et al., 2007) and in particular, DWI in conjunction with DCE, has shown ability to discriminate different areas within highly heterogeneous head and neck lesions (Wang et al., 2012a, Powell et al., 2013). This shows promise as a method to identify radio-resistant disease for dose-boosting, and is currently the target of several studies.

The advantages of the superior contrast provided by MRI also apply to spine and para-spinal tumours and metastases (Thariat et al., 2009, Bedford et al., 2012). T2-weighted MR images provide good contrast between the spinal cord and the surrounding CSF, while T1-weighted images usually provide the best visualisation of spinal tumours, particularly after contrast agent administration. The development of Intensity Modulated RT (IMRT) and Volumetric Modulated Arc Therapy (VMAT) has enabled treatment of lesions in proximity to the spine, and the accurate outlining of this organ at risk for minimising radiation dose is essential. In order to achieve confidence in the CT-MR registration it is usual to include at least one vertebra above and one vertebra below the site of disease in the MR examination volume. This approach definitely requires a flat bed, with thermoplastic fixation device for the cervical spine (which is most mobile), and MR-compatible positioning devices for inferior portions of the spine.

In some cases spinal metastases are stabilised with the use of metallic fixation devices, which degrade image quality of MR and CT examinations (FIGURE 11 spine+metal). For lesions located in the vicinity of metallic implants, it may be advantageous to employ MR techniques for metal artifact reduction (Panek et al., 2013). Although the degree of confidence in the CT-MR fusion increases as the artifacts are restricted to a smaller volume, further work is required to validate this approach and quantify its benefits.

Prostate

The main role of MRI in prostate radiotherapy planning is for outlining of the prostate, intraprostatic lesions, and involved nodes, in the treatment of localised prostate cancer. The good soft-tissue contrast of MRI gives good delineation of the prostate gland and neighbouring critical structures (bladder and rectum). Implanted gold seeds are often used for position verification and interfraction displacement reduction (van der Heide et al., 2007), but they are also useful for co-registering the MRI data to a planning CT scan (Huisman et al., 2005, Parker et al., 2003).

Prostate cancer is relatively unusual in that histological slices from patients with prostate cancer usually show several foci of disease, rather than a single tumour as is common for most other cancers. Not all of these are clinically significant. While significant effort is being made into identifying the dominant intraprostatic lesion for targeting boost radiation doses (Nutting et al., 2002, Li et al., 2005) it is still essential to irradiate the whole prostate. Several studies have demonstrated the theoretical improvements to be expected using such boost doses (Onal et al., 2014, Riches et al., 2014, Xia et al., 2001), and have shown that an integrated strategy is more efficient and effective than planning the uniform dose and a boost dose separately (Li et al., 2005). A number of trials are under way to investigate the optimal boost. The clinical efficacy also remains to be established (Bauman et al., 2013).

Sometimes none of the prostate cancer foci detected are clinically significant. To avoid unnecessary treatment-related morbidity a key question is therefore to identify the cancers that need treating. Currently patients with low risk prostate cancers are offered Active Surveillance, in which the tumour is monitored but treatment is only given if progression is detected. Criteria for low risk generally include tumor stage (T1c or T2a), a PSA value of < 10 ug/l, a Gleason score of ≤ 6 , and limited extent of disease on biopsy (Ganz et al., 2012). Surprisingly tumour size as detected by imaging is not in this list, but is proposed (van den Bergh et al., 2014).

While prostate cancer is generally seen as lower signal intensity than normal prostate in T2w MR images (especially in the peripheral zone, where 70% of prostate cancers arise) other pathologies may also have this appearance. It is therefore helpful to acquire MR images with additional types of contrast to increase the specificity for diagnosis. The most widely investigated multiparametric MRI methods shown to be of value in prostate are DWI (increased cellularity of tumours results in a lower ADC and higher signals on diffusion-weighted images), dynamic contrast-enhanced MRI, and magnetic resonance spectroscopic imaging. Since prostate cancer is one of the few cancers for which good validation against histology is possible, owing to the widespread use of prostatectomy for treatment of organ-confined disease, there are a large number of papers measuring the sensitivity and specificity

of the different techniques in different cohorts (Tamada et al., 2008, Futterer et al., 2006, Riches et al., 2009b). The optimal combination is not yet agreed. A scheme called PI-RADS (Prostate Imaging Reporting and Data System, (Barentsz et al., 2012) has recently been proposed for reporting multiparametric MRI. In this scheme each of T2w, DWI, DCE-MRI and MRSI (when included) are scored on a scale of 1-5; higher total scores correspond to a higher certainty of clinically significant cancer being present. This approach is showing significant promise for harmonising the reporting, but is still relatively young and significant revisions may be anticipated.

All multiparametric MRI methods are improved by the use of an endo-rectal MRI receiver coil (ideally inflated with perfluorocarbon rather than air to avoid a large discontinuity in magnetic susceptibility (Choi and Ma, 2008)), but with the penalty of distorting the prostate and making the registration of the prostate more challenging. When neo-adjuvant hormone therapy is used to shrink the tumour prior to radiotherapy this both shrinks the prostate (Nishiyama et al., 2004) and reduces the contrast in various MRI modalities (Padhani et al., 2001, Mueller-Lisse et al., 2007). For boosting doses to the dominant lesion it will therefore be necessary to identify it prior to hormone treatment, and then to estimate the effect of shrinkage (Riches et al., 2009a).

Owing to the better tissue contrast, MRI has been shown to reduce the target volume by about 30% compared with CT (Rasch et al., 1999). Using the MRI-defined target volume has led to comparable outcomes, with similar overall survival and PSA relapse-free survival. It has however produced reduced side-effects (Sander et al., 2013). MRI can also upstage cancers in a number of cases, thereby requiring extracapsular extension or seminal vesicle invasion to be included in the radiotherapy plan (Chang et al., 2014). A further advantage of MRI is that it can be used to delineate the urethral track for sparing in the treatment plan.

Transrectal ultrasound (TRUS) is currently the imaging modality of choice for prostate brachytherapy planning and guidance but both high resolution MRI performed with an endorectal receiver coil and conventional MRI have been explored. Albert et al. (2013) reported smaller dimensions for the prostate in MRI compared with those measured using TRUS. Some of the discrepancy is attributed to distortion of the anatomy caused by the endorectal coil, but the higher contrast between prostate and surrounding tissues in MRI is also acknowledged. Differences in dimensions have a clear implication for dose determination at the prostate margins (Crook et al., 2010). T2W sequences are usually preferred for prostate imaging and this also applies to brachytherapy planning (Bowes et al., 2013). MRI has also been used after seed implantation for dosimetry purposes (Ohashi et al., 2012); Katayama et al. (2011) combined T2W and T2*W images to visualise both lesions and seeds. MRI-based dosimetry proves particularly valuable in the presence of calcifications, and contributes towards integration of brachytherapy and external beam RT.

Gynaecological Cancers

In the last 15 years the treatment of gynaecological cancers has moved away from the conventional four field external beam RT to more conformal techniques, enabled by the introduction of 3D imaging, initially CT, and more recently MRI (Barkati et al., 2010, Wanderas et al., 2012, Weitmann et al., 2005). Current treatment standards involve external

beam RT often followed by brachytherapy, and an integrated approach to volume dosimetry (Potter et al., 2006). In brachytherapy high dose rates require better tissue contrast to optimise target delineation and the sparing of organs at risk (bladder, vagina, rectum and sigmoid colon), which are better delineated with MRI (Barillot and Reynaud-Bougnoux, 2006, Dolezel et al., 2012, Eskander et al., 2010, Wanderas et al., 2012). The advantages of using MRI are more pronounced for smaller tumours (Zwahlen et al., 2009). MR-CT registration has been shown to be feasible (Kim et al., 2014), and although the paucity of studies involving histological validation is noted (de Boer et al., 2013), the benefit of T₂-weighted MRI has been demonstrated (Dimopoulos et al., 2012). The GTV is often larger on CT images compared with MRI (Viswanathan et al., 2007). The Gynaecological GEC-ESTRO Working Group recommended both a conventional MRI pelvic examination prior to RT and a MRI Brachytherapy examination, with the applicator in place for cervix cancers (Dimopoulos et al., 2012). Gynaecological cancer is expected to respond well to RT, and as a result significant differences are expected between MR images acquired at diagnosis and for brachytherapy planning (Haie-Meder et al., 2005). The use of a single MR examination was also investigated because multiple MRI examinations are not necessarily available at all RT centres (Tan, 2011). In addition, Taylor and Powell (2008) used MRI to assess gynaecological inter-fractional motion, shown to be affected by bladder and rectal filling, and proposed asymmetrical margins for the CTV-PTV expansion of the uterus, cervix and vagina.

Brachytherapy is used to treat cervix, uterus and vaginal tumours with a number of MR-compatible intra-cavitary and interstitial applicators⁵. These are mostly plastic devices which appear in the MR images as a signal void (Figure 12). The applicators have indentations and internal structures to enable the user to locate their position accurately in three dimensions. The knowledge of the position of the applicator tip in the superior/inferior direction is essential for planning, and so is the angle of rotation around the superior/inferior axis. High resolution 3D T₂-weighted imaging is considered advantageous, as the applicator geometry favours outlining volumes in the sagittal orientation (Radawski et al., 2012).

The MRI brachytherapy planning examination involves many logistic difficulties. The MR examination occurs after patient recovery from the insertion of the brachytherapy applicator under general anaesthetic. The treatment delivery must start on the same day, thus imposing constraints on the time allowed for treatment planning. MRI examination employs a bladder filling protocol to reproduce the treatment position and muscle relaxants to reduce bowel motion, thus preserving image quality.

In gynaecological brachytherapy the radiation source is placed in close proximity to the lesion, inside an applicator. Assuming that all soft tissues have the same electron density, it is in principle possible to plan brachytherapy from MR images only. This approach removes the need for a CT examination with the applicator in situ, which also would have to take place on the same day of applicator insertion, prior to treatment planning.

⁵https://www.varian.com/sites/default/files/resource_attachments/Brachytherapy_GYN_Applicator_Catalog.pdf
<http://www.elekta.com/healthcare-professionals/products/elekta-brachytherapy/applicators/gyn.html>

Rectal Cancer

Rectal cancer has been the most common target of MRI in RT planning for cancers of the digestive tract. Although MRI produces high-quality images with better contrast resolution than CT, its use in RT planning is limited by physiological motion. While diagnostic MRI is often undertaken with the use of a muscle relaxant, rectal imaging is still affected by bladder filling and rectal distension, and benefits from standardisation of patient preparation between MRI and CT planning examinations. Inter-fraction motion has been studied using cone-beam CT, and displacement was shown to be most prominent in the upper rectum (Chong et al., 2011).

Both T2-weighted and contrast-enhanced T1-weighted MRI sequences have been used to outline rectal tumours (Roels et al., 2009, Braendengen et al., 2011), (Tan et al., 2010, O'Neill et al., 2009). Studies of MRI in rectal RT planning on a relatively small number of patients suggest that the GTV delineated using only MR images is smaller than that delineated using CT only (Tan et al., 2010, Shihab et al., 2009), and that MRI has a greater impact on the GTV delineation in cases of involvement of the sigmoid and anorectal regions (Tan et al., 2010). These results are significant, and rectal MRI for RT planning needs evaluating in larger cohorts, as smaller GTVs may lead to smaller PTVs and subsequent reduction of the dose delivered to organs at risk and toxicity.

Liver

In common with all organs in the abdomen and chest, the liver suffers from significant respiratory motion. Various methods have been developed to address this, including breath-holding, respiratory triggering, and active breathing control, which can reduce the error to about 5 mm (Yu et al., 2013). Adapting margins of the PTV according to the extent of individual breathing motion as measured by 4DCT or MRI is also used (Brock and Dawson, 2010). Modelling of liver motion to produce radiotherapy plans to reduce the effects of motion have been investigated (White et al., 2009, Hawkins et al., 2009) but have not moved into clinical practice. In the future one important application of MR-linacs (see below) will be to help gate liver motion and therefore reduce the margins required.

For treatment planning of liver metastases, MRI has been shown to identify substantially larger tumour volumes compared with CT, with the target volume increasing by 180% for T1w-MRI, 178% for contrast-enhanced T1w-MRI, and 246% for T2w MRI (Pech et al., 2008). Concordance between MRI and CT has been assessed as about 60-80% (Voroney et al., 2006).

The main “organ at risk” is liver itself, with liver toxicity limiting the maximum radiation dose. Some studies have started investigating functional imaging to evaluate this damage (Partridge et al., 2010) but results are preliminary as yet.

MR-guided tumour ablation using brachytherapy has been attempted, using a 1 tesla open MRI system (Ricke et al., 2010). With a median intervention time of 61 minutes 218 of 224 tumours were completely obliterated with only 4% minor complications.

Lung

Lung lesions can be both displaced and deformed by respiratory motion. In lung cancer MRI has been used to assess the range of GTV motion in three-dimensions. The low proton density of healthy lung parenchyma yields low image intensity in MRI and ensures good contrast between tumour and surrounding lung parenchyma. Motion assessment is most successful in sequences that allow good visualisation of blood vessels within the lung, as those provide useful references for tumour position. Both balanced steady-state gradient-echo sequences and EPI sequences have been used for this purpose (Blackall et al., 2006, Plathow et al., 2004a, Plathow et al., 2004b).

Lung RT can be delivered during breath-holds if the degree of lung inflation is kept constant between fractions. In this context, MR images must be acquired under the same conditions to be useful. Our group has successfully adapted an Active Breathing Co-ordinator to work within the MRI scanner and keep a constant level of lung inflation between consecutive breath-holds (Kaza et al., 2015). This device is currently under clinical evaluation for curative lung patients.

If lung RT is delivered during breathing using motion tracking devices, a model is required to correlate the motion of the GTV to the tracking of either chest wall position or inspiration volume (Koch et al., 2004, Liu et al., 2004). The accuracy of RT delivery will therefore depend on the quality of the model, which must therefore be validated. Variations in performance at different tumour sites are expected.

An additional contribution of lung MRI to RT planning is the use of hyperpolarised gases to detect the volume of lung parenchyma which is actually functional (Ireland et al., 2007). Although this technique is expensive and not widely available, it can provide valuable information for RT planning, enabling the sparing of the parts of the lung which remain functional.

Breast

In breast cancer radiotherapy is mainly used in association with mastectomy or breast-conserving surgery in early disease. The whole breast may be irradiated, or either the whole or partial breast and the tumor bed may be boosted using IMRT. While historically whole breast irradiation was used, accelerated partial-breast irradiation is now an option for early breast cancer (Smith et al., 2009). Imaging methods to delineate the tumour bed for this purpose (including MRI) have recently been reviewed by Yang et al (2013). In general external beam radiotherapy is used, although brachytherapy also has a role (Hepel and Wazer, 2012), using radioactive wires or a small source.

Generally MRI of the breast is performed prone; thus planning scans will need to be performed in the suboptimal supine position in order to match that for treatment. Given the highly deformable nature of the breast tools have to be developed for co-registering MRI and planning CT scans (Yang et al., 2012).

While MRI has better soft tissue contrast in comparison with CT, its role in radiotherapy planning is relatively limited. In 2009 a review concluded that there was little evidence to

support the routine use of preoperative MRI in terms of surgical care or prognosis (Houssami and Hayes, 2009). For preoperative target volume delineation, MRI yields a larger CTV than CT, with more irregular and speculated margins (den Hartogh et al., 2014) or a smaller CTV (Jolicoeur et al., 2011, Mast et al., 2014). MRI to CT co-registration does not significantly alter the concordance between readers (Mast et al., 2014). Definition of the post-surgical tumour bed appears to yield a smaller volume with MR and with better inter-observer variability (Jolicoeur et al., 2011), although another study has shown that MRI adds little to CT for definition of the lumpectomy cavity (Giezen et al., 2011). Generally clips are placed in the tumour bed to aid identification using CT, but these are not well visualised by MRI. When it has been possible to compare with histology, one study has shown that MRI underestimated in 15% and overestimated in 33% of cases (although most of these had additional findings outside the main lesion (Grimsby et al., 2009)). Another study has shown subclinical disease in specimens at >20mm from the MRI GTV (Schmitz et al., 2010) demonstrating the need for significant margins.

Real-Time Image Guided RT

For relatively mobile tissues and structures there is advantage in real-time tracking of motion to increase the accuracy of radiotherapy delivery. Although the contrast of X-Ray images is in most cases not suited to tracking cancer, X-Ray tracking of the tumour bed can be enabled by implanting metallic markers in the vicinity of the lesion. X-Ray technology has enabled 3D tracking by using two orthogonal images. X-Ray guided RT is a clinical tool, often used in abdominal examinations (Cyberknife, Accuray, Sunnyville, California⁶; Figure 13). Other real time tracking techniques make use of ultrasound guidance, for guiding prostate RT for example, exploiting ultrasound's ability to detect the prostate through the rectal wall⁷. MRI is often used in conjunction with these techniques, registered with the planning CT.

A separate approach is to implant active markers such as transponders which report their position to dedicated systems using, for example, a resonant circuit (Zhu et al., 2009). The transponders are small and do not interfere with the RT delivery. Although it may be desirable to add MRI to the workflow for patients treated with a transponder-based RT guidance, the current technology produces MR-safe devices which are not entirely MR-compatible. Transponders cause significant signal loss to the vicinity by containing ferromagnetic materials, limiting their value in MRI examinations.

Combined MRI and RT Systems

The ultimate in real-time image guidance would be provided by the simultaneous acquisition of MR images during treatment. This would not only allow lesion movement to be followed, but also permit some reduction of the large margins generally introduced in the PTV around the CTV to allow for movement, daily position variations, and tissue changes in response to the radiation. Monitoring the position of bony anatomy and fiducial markers on a daily basis using Image-guided Radiotherapy (IGRT) partly resolves this problem, but the cone-beam

⁶http://www.accuray.com/sites/default/files/ck_m6_series_brochure_en_501004b.pdf

⁷http://www.elekta.com/healthcare-professionals/products/elekta-software/clarity.html?utm_source=clarity&utm_medium=redirect&utm_campaign=redirects

CT or megavoltage CT methods currently used lack the soft tissue contrast required. Integrating MRI functionality with an accelerator has been a goal of developers for many years and has now reached the prototype stage.

At the University Medical Center in Utrecht a 1.5T Philips MRI scanner is being integrated with an Elekta 6 MV radiotherapy accelerator (Legendijk et al., 2008). In the US a 0.35T open MRI system is being combined with a 60Cobalt radiotherapy system⁸, while in Canada at the Cross Cancer Institute a prototype system has been built in which a permanent magnet 0.2T MRI has been combined with a 6 MV accelerator (Fallone et al., 2009).

Apart from the requirement for an aperture to enable the radiotherapy beam to enter the magnet, challenges to be overcome include avoiding the effect of the magnetic field on the accelerator, and of magnetic distortions and noise from the accelerator on the MR images. In addition the electron return effect gives increased skin dose in the presence of a magnetic field. The significance of this has been evaluated for some specific situations. For example it has been calculated to increase the skin dose for whole breast irradiation, but have a negligible impact for partial breast irradiation (van Heijst, 2013). Developments in this field have recently been reviewed in more detail (Legendijk et al., 2014).

Summary

The improved tumour delineation available with MRI compared with CT is slowly making its way into clinical practice, as MRI scanners become more widely available to RT planning. In general a planning CT scan is still used to enable calculation of electron density for dose calculations, with registration required between the MR and the CT scans. This is clearly most readily achieved in rigid structures like the head, but is also making progress for other applications, using anatomical landmarks or implanted seeds to aid image co-registration. It may be anticipated that radiotherapy planning software will soon be able to take full advantage of the range of image contrast and orientations available with MRI. The advent of combined MR-linac systems, currently under development, will enable new paradigms for image-guided radiotherapy to be opened up, with the potential for true real-time guidance becoming possible.

Acknowledgements

We thank Dr Vibeke Hansen from the Royal Marsden Hospital for careful reading of the manuscript, leading to many helpful suggestions. We gratefully acknowledge funding from Cancer Research UK in association with the MRC and Department of Health (England) grant C1060/A10334, and NHS funding to the NIHR Biomedical Research Centre and Clinical Research Facility.

Figure Acknowledgements: The authors wish to thank Dr Vibeke Hansen, Dr Margaret Bidmead and staff in the departments of Radiotherapy and Radiology, in particular the following: Chris South (Figure 1 and Figure 8), Rafal Panek (Figures 3b, 6, 11), Kate Newbold, Marco Borri, James D'Arcy (Figures 3b and 6), Ian Murray (Figure 6), Vibeke Hansen (Figure 9), Anna Kirby (Figure 10), Jamie Dean and Siemens Medical Systems (Figure 11), Caroline Lamb, Susan Lalondrelle, Georgina Hopkinson (Figure 12), Emma Wells (Figure 13).

⁸www.viewray.com

References

- Ahmed M, Schmidt M, Sohaib A, Kong C, Burke K, Richardson C, Usher M, Brennan S, Riddell A, Davies M, Newbold K, et al. The value of magnetic resonance imaging in target volume delineation of base of tongue tumours--a study using flexible surface coils. *Radiother Oncol.* 2010; 94:161–7. [PubMed: 20096947]
- Albert JM, Swanson DA, Pugh TJ, Zhang M, Bruno TL, Kudchadker RJ, Frank SJ. Magnetic resonance imaging-based treatment planning for prostate brachytherapy. *Brachytherapy.* 2013; 12:30–7. [PubMed: 22727474]
- Andersson JL, Skare S. A model-based method for retrospective correction of geometric distortions in diffusion-weighted EPI. *Neuroimage.* 2002; 16:177–99. [PubMed: 11969328]
- Ardenjaer-Larsen JH, Fridlund B, Gram A, Hansson G, Hansson L, Lerche MH, Servin R, Thaning M, Golman K. Increase in signal-to-noise ratio of > 10,000 times in liquid-state NMR. *Proc Natl Acad Sci U S A.* 2003; 100:10158–63. [PubMed: 12930897]
- Arias-Mendoza F, Payne GS, Zakian K, Stubbs M, O'connor OA, Mojahed H, Smith MR, Schwarz AJ, Shukla-Dave A, Howe F, Poptani H, et al. Noninvasive phosphorus magnetic resonance spectroscopic imaging predicts outcome to first-line chemotherapy in newly diagnosed patients with diffuse large B-cell lymphoma. *Acad Radiol.* 2013; 20:1122–9. [PubMed: 23931426]
- Ashby, FG. *Statistical Analysis of fMRI Data.* MIT Press; 2011.
- Aslian H, Sadeghi M, Mahdavi SR, Babapour Mofrad F, Astarakee M, Khaledi N, Fadavi P. Magnetic resonance imaging-based target volume delineation in radiation therapy treatment planning for brain tumors using localized region-based active contour. *Int J Radiat Oncol Biol Phys.* 2013; 87:195–201. [PubMed: 23920396]
- Baldwin LN, Wachowicz K, Thomas SD, Rivest R, Fallone BG. Characterization, prediction, and correction of geometric distortion in 3 T MR images. *Med Phys.* 2007; 34:388–99. [PubMed: 17388155]
- Barentsz JO, Richenberg J, Clements R, Choyke P, Verma S, Villeirs G, Rouviere O, Logager V, Futterer JJ, European Society of Urogenital, R. ESUR prostate MR guidelines 2012. *Eur Radiol.* 2012; 22:746–57. [PubMed: 22322308]
- Barillot I, Reynaud-Bougnoix A. The use of MRI in planning radiotherapy for gynaecological tumours. *Cancer Imaging.* 2006; 6:100–6. [PubMed: 16829471]
- Barkati M, Van Dyk S, Foroudi F, Narayan K. The use of magnetic resonance imaging for image-guided brachytherapy. *J Med Imaging Radiat Oncol.* 2010; 54:137–41. [PubMed: 20518877]
- Bauman G, Haider M, Van der Heide UA, Menard C. Boosting imaging defined dominant prostatic tumors: a systematic review. *Radiother Oncol.* 2013; 107:274–81. [PubMed: 23791306]
- Bedford JL, Convery HM, Hansen VN, Saran FH. Paraspinal volumetric modulated arc therapy. *Br J Radiol.* 2012; 85:1128–33. [PubMed: 22215885]
- Bhide SA, Ahmed M, Barbachano Y, Newbold K, Harrington KJ, Nutting CM. Sequential induction chemotherapy followed by radical chemo-radiation in the treatment of locoregionally advanced head-and-neck cancer. *Br J Cancer.* 2008; 99:57–62. [PubMed: 18560402]
- Blackall JM, Ahmad S, Miquel ME, McClelland JR, Landau DB, Hawkes DJ. MRI-based measurements of respiratory motion variability and assessment of imaging strategies for radiotherapy planning. *Phys Med Biol.* 2006; 51:4147–69. [PubMed: 16912374]
- Bowes D, Crook JM, Rajapakshe R, Araujo C, Parker B. Defining a magnetic resonance scan sequence for permanent seed prostate brachytherapy postimplant assessment. *Brachytherapy.* 2013; 12:25–9. [PubMed: 22513105]
- Braendengen M, Hansson K, Radu C, Siegbahn A, Jacobsson H, Glimelius B. Delineation of gross tumor volume (GTV) for radiation treatment planning of locally advanced rectal cancer using information from MRI or FDG-PET/CT: a prospective study. *Int J Radiat Oncol Biol Phys.* 2011; 81:e439–45. [PubMed: 21641122]
- Brix L, Ringgaard S, Sorensen TS, Poulsen PR. Three-dimensional liver motion tracking using real-time two-dimensional MRI. *Med Phys.* 2014; 41 042302.
- Brock KK, Dawson LA. Adaptive management of liver cancer radiotherapy. *Semin Radiat Oncol.* 2010; 20:107–15. [PubMed: 20219548]

- Buis DR, Lagerwaard FJ, Dirven CM, Barkhof F, Knol DL, van den Berg R, Slotman BJ, Vandertop WP. Delineation of brain AVMs on MR-Angiography for the purpose of stereotactic radiosurgery. *Int J Radiat Oncol Biol Phys.* 2007; 67:308–16. [PubMed: 17189079]
- Burgos N, Cardoso MJ, Modat M, Pedemonte S, Dickson J, Barnes A, Duncan JS, Atkinson D, Arridge SR, Hutton BF, Ourselin S. Attenuation correction synthesis for hybrid PET-MR scanners. *Med Image Comput Comput Assist Interv.* 2013; 16:147–54.
- Butts K, Pauly JM, Gold GE. Reduction of blurring in view angle tilting MRI. *Magn Reson Med.* 2005; 53:418–24. [PubMed: 15678535]
- Calamante F. Perfusion MRI using dynamic-susceptibility contrast MRI: quantification issues in patient studies. *Top Magn Reson Imaging.* 2010; 21:75–85. [PubMed: 21613873]
- Calcerrada Diaz-Santos N, Blasco Amaro JA, Cardiel GA, Andradas Aragonés E. The safety and efficacy of robotic image-guided radiosurgery system treatment for intra- and extracranial lesions: a systematic review of the literature. *Radiother Oncol.* 2008; 89:245–53. [PubMed: 18760852]
- Callaghan, PT. Principles of Nuclear Magnetic Resonance Microscopy. Clarendon Press; 1991.
- Caramanos Z, Fonov VS, Francis SJ, Narayanan S, Pike GB, Collins DL, Arnold DL. Gradient distortions in MRI: characterizing and correcting for their effects on SIENA-generated measures of brain volume change. *Neuroimage.* 2010; 49:1601–11. [PubMed: 19682586]
- Chang H, Fitzpatrick JM. A technique for accurate magnetic resonance imaging in the presence of field inhomogeneities. *IEEE Trans Med Imaging.* 1992; 11:319–29. [PubMed: 18222873]
- Chang JH, Lim Joon D, Nguyen BT, Hiew CY, Esler S, Angus D, Chao M, Wada M, Quong G, Khoo V. MRI scans significantly change target coverage decisions in radical radiotherapy for prostate cancer. *J Med Imaging Radiat Oncol.* 2014; 58:237–43. [PubMed: 24690247]
- Choi H, Ma J. Use of perfluorocarbon compound in the endorectal coil to improve MR spectroscopy of the prostate. *AJR Am J Roentgenol.* 2008; 190:1055–9. [PubMed: 18356455]
- Creak AL, Tree A, Saran F. Radiotherapy planning in high-grade gliomas: a survey of current UK practice. *Clin Oncol (R Coll Radiol).* 2011; 23:189–98. [PubMed: 21288703]
- Crook J, Patil N, Ma C, Mclean M, Borg J. Magnetic resonance imaging-defined treatment margins in iodine-125 prostate brachytherapy. *Int J Radiat Oncol Biol Phys.* 2010; 77:1079–84. [PubMed: 19879700]
- Cusack R, Brett M, Osswald K. An evaluation of the use of magnetic field maps to undistort echo-planar images. *Neuroimage.* 2003; 18:127–42. [PubMed: 12507450]
- D'arcy JA, Collins DJ, Padhani AR, Walker-Samuel S, Suckling J, Leach MO. Informatics in Radiology (infoRAD): Magnetic Resonance Imaging Workbench: analysis and visualization of dynamic contrast-enhanced MR imaging data. *Radiographics.* 2006; 26:621–32. [PubMed: 16549620]
- de Boer P, Adam JA, Buist MR, van de Vijver MJ, Rasch CR, Stoker J, Bipat S, Stalpers LJ. Role of MRI in detecting involvement of the uterine internal os in uterine cervical cancer: systematic review of diagnostic test accuracy. *Eur J Radiol.* 2013; 82:e422–8. [PubMed: 23711423]
- de Graaf, RA. *In vivo NMR Spectroscopy.* John Wiley; 2007.
- Delso G, Furst S, Jakoby B, Ladebeck R, Ganter C, Nekolla SG, Schwaiger M, Ziegler SI. Performance measurements of the Siemens mMR integrated whole-body PET/MR scanner. *J Nucl Med.* 2011; 52:1914–22. [PubMed: 22080447]
- den Hartogh MD, Philippens ME, van Dam IE, Kleynen CE, Tersteeg RJ, Pijnappel RM, Kotte AN, Verkooijen HM, van den Bosch MA, van Vulpen M, van Asselen B, et al. MRI and CT imaging for preoperative target volume delineation in breast-conserving therapy. *Radiat Oncol.* 2014; 9:63. [PubMed: 24571783]
- Dimopoulos JC, Petrow P, Tanderup K, Petric P, Berger D, Kirisits C, Pedersen EM, Van Limbergen E, Haie-Meder C, Potter R. Recommendations from Gynaecological (GYN) GEC-ESTRO Working Group (IV): Basic principles and parameters for MR imaging within the frame of image based adaptive cervix cancer brachytherapy. *Radiother Oncol.* 2012; 103:113–22. [PubMed: 22296748]
- Dolezel M, Odrázka K, Zizka J, Vanasek J, Kohlova T, Kroulik T, Spitzer D, Ryska P, Tichy M, Kostal M, Jalcova L. MRI-based preplanning using CT and MRI data fusion in patients with cervical cancer treated with 3D-based brachytherapy: feasibility and accuracy study. *Int J Radiat Oncol Biol Phys.* 2012; 84:146–52. [PubMed: 22300570]

- Dong Y, Chang Z, Xie G, Whitehead G, Ji JX. Susceptibility-based positive contrast MRI of brachytherapy seeds. *Magn Reson Med*. 2014
- Doran SJ, Charles-Edwards L, Reinsberg SA, Leach MO. A complete distortion correction for MR images: I. Gradient warp correction. *Phys Med Biol*. 2005; 50:1343–61. [PubMed: 15798328]
- Eskander RN, Scanderbeg D, Saenz CC, Brown M, Yashar C. Comparison of computed tomography and magnetic resonance imaging in cervical cancer brachytherapy target and normal tissue contouring. *Int J Gynecol Cancer*. 2010; 20:47–53. [PubMed: 20130502]
- Fallone BG, Murray B, Rathee S, Stanescu T, Steciw S, Vidakovic S, Blosser E, Tymofichuk D. First MR images obtained during megavoltage photon irradiation from a prototype integrated linac-MR system. *Med Phys*. 2009; 36:2084–8. [PubMed: 19610297]
- Farace P, Giri MG, Meliado G, Amelio D, Widesott L, Ricciardi GK, Dall'Oglio S, Rizzotti A, Sbarbati A, Beltramello A, Maluta S, et al. Clinical target volume delineation in glioblastomas: pre-operative versus post-operative/pre-radiotherapy MRI. *Br J Radiol*. 2011; 84:271–8. [PubMed: 21045069]
- Ferl GZ, Port RE. Quantification of antiangiogenic and antivascular drug activity by kinetic analysis of DCE-MRI data. *Clin Pharmacol Ther*. 2012; 92:118–24. [PubMed: 22588603]
- Fiorentino A, Caivano R, Pedicini P, Fusco V. Clinical target volume definition for glioblastoma radiotherapy planning: magnetic resonance imaging and computed tomography. *Clin Transl Oncol*. 2013; 15:754–8. [PubMed: 23359180]
- Flickinger JC, Lunsford LD, Kondziolka D. Dose prescription and dose-volume effects in radiosurgery. *Neurosurg Clin N Am*. 1992; 3:51–9. [PubMed: 1633452]
- Futterer JJ, Heijmink SW, Scheenen TW, Veltman J, Huisman HJ, Vos P, Hulsbergen-Van de Kaa CA, Witjes JA, Krabbe PF, Heerschap A, Barentsz JO. Prostate cancer localization with dynamic contrast-enhanced MR imaging and proton MR spectroscopic imaging. *Radiology*. 2006; 241:449–58. [PubMed: 16966484]
- Gaertner FC, Furst S, Schwaiger M. PET/MR: a paradigm shift. *Cancer Imaging*. 2013; 13:36–52. [PubMed: 23446110]
- Ganz PA, Barry JM, Burke W, Col NF, Corso PS, Dodson E, Hammond ME, Kogan BA, Lynch CF, Newcomer L, Seifter EJ, et al. National Institutes of Health State-of-the-Science Conference: role of active surveillance in the management of men with localized prostate cancer. *Ann Intern Med*. 2012; 156:591–5. [PubMed: 22351514]
- Giezen M, Kouwenhoven E, Scholten AN, Coerkamp EG, Heijenbrok M, Jansen WP, Mast ME, Petoukhova AL, Struikmans H. Magnetic resonance imaging- versus computed tomography-based target volume delineation of the glandular breast tissue (clinical target volume breast) in breast-conserving therapy: an exploratory study. *Int J Radiat Oncol Biol Phys*. 2011; 81:804–11. [PubMed: 20843611]
- Glunde K, Bhujwala ZM, Ronen SM. Choline metabolism in malignant transformation. *Nat Rev Cancer*. 2011a; 11:835–48. [PubMed: 22089420]
- Glunde K, Jiang L, Moestue SA, Gribbestad IS. MRS and MRSI guidance in molecular medicine: targeting and monitoring of choline and glucose metabolism in cancer. *NMR Biomed*. 2011b; 24:673–90. [PubMed: 21793073]
- Grimbsy GM, Gray R, Dueck A, Carpenter S, Stucky CC, Aspey H, Giurescu ME, Pockaj B. Is there concordance of invasive breast cancer pathologic tumor size with magnetic resonance imaging? *Am J Surg*. 2009; 198:500–4. [PubMed: 19800455]
- Haacke, EM.; Brown, RW.; Thompson, MR.; Venkatesan, R. *Magnetic Resonance Imaging*. Wiley-Liss; 1999.
- Haie-Meder C, Potter R, van Limbergen E, Briot E, De Brabandere M, Dimopoulos J, Dumas I, Hellebust TP, Kirisits C, Lang S, Muschitz S, et al. Recommendations from Gynaecological (GYN) GEC-ESTRO Working Group (I): concepts and terms in 3D image based 3D treatment planning in cervix cancer brachytherapy with emphasis on MRI assessment of GTV and CTV. *Radiother Oncol*. 2005; 74:235–45. [PubMed: 15763303]
- Hambrock T, Somford DM, Huisman HJ, van Oort IM, Witjes JA, Hulsbergen-van de Kaa CA, Scheenen T, Barentsz JO. Relationship between apparent diffusion coefficients at 3.0-T MR

- imaging and Gleason grade in peripheral zone prostate cancer. *Radiology*. 2011; 259:453–61. [PubMed: 21502392]
- Hargreaves BA, Worters PW, Pauly KB, Pauly JM, Koch KM, Gold GE. Metal-induced artifacts in MRI. *AJR Am J Roentgenol*. 2011; 197:547–55. [PubMed: 21862795]
- Harnan SE, Cooper KL, Meng Y, Ward SE, Fitzgerald P, Papaioannou D, Ingram C, Lorenz E, Wilkinson ID, Wyld L. Magnetic resonance for assessment of axillary lymph node status in early breast cancer: a systematic review and meta-analysis. *Eur J Surg Oncol*. 2011; 37:928–36. [PubMed: 21855267]
- Hartung MP, Grist TM, Francois CJ. Magnetic resonance angiography: current status and future directions. *J Cardiovasc Magn Reson*. 2011; 13:19. [PubMed: 21388544]
- Hawkins M, Bedford JL, Warrington AP, Coolens C, Tait D. VMAT Compared with Gated Highly Conformal Optimization for Dose Escalation in Partial Liver Radiotherapy. *Int J Radiat Oncol Biol Phys*. 2009; 75:S121–S122.
- Hepel JT, Wazer DE. A comparison of brachytherapy techniques for partial breast irradiation. *Brachytherapy*. 2012; 11:163–75. [PubMed: 21816686]
- Houssami N, Hayes DF. Review of preoperative magnetic resonance imaging (MRI) in breast cancer: should MRI be performed on all women with newly diagnosed, early stage breast cancer? *CA Cancer J Clin*. 2009; 59:290–302. [PubMed: 19679690]
- Howe FA, Barton SJ, Cudlip SA, Stubbs M, Saunders DE, Murphy M, Wilkins P, Opstad KS, Doyle VL, McLean MA, Bell BA, Griffiths JR. Metabolic profiles of human brain tumors using quantitative in vivo 1H magnetic resonance spectroscopy. *Magn Reson Med*. 2003; 49:223–32. [PubMed: 12541241]
- Huettel, SA.; Song, AW.; Mccarthy, G. *Functional magnetic resonance imaging*. Massachusetts: Sinauer; 2009.
- Huisman HJ, Futterer JJ, van Lin EN, Welmers A, Scheenen TW, van Dalen JA, Visser AG, Witjes JA, Barentsz JO. Prostate cancer: precision of integrating functional MR imaging with radiation therapy treatment by using fiducial gold markers. *Radiology*. 2005; 236:311–7. [PubMed: 15983070]
- Ireland RH, Bragg CM, Mcjury M, Woodhouse N, Fichelle S, van Beek EJ, Wild JM, Hatton MQ. Feasibility of image registration and intensity-modulated radiotherapy planning with hyperpolarized helium-3 magnetic resonance imaging for non-small-cell lung cancer. *Int J Radiat Oncol Biol Phys*. 2007; 68:273–81. [PubMed: 17448880]
- Jagsi R, Moran JM, Kessler ML, Marsh RB, Balter JM, Pierce LJ. Respiratory motion of the heart and positional reproducibility under active breathing control. *Int J Radiat Oncol Biol Phys*. 2007; 68:253–8. [PubMed: 17448878]
- Jahan N, Narayanan P, Rockall A. Magnetic resonance lymphography in gynaecological malignancies. *Cancer Imaging*. 2010; 10:85–96. [PubMed: 20233680]
- Janke A, Zhao H, Cowin GJ, Galloway GJ, Doddrell DM. Use of spherical harmonic deconvolution methods to compensate for nonlinear gradient effects on MRI images. *Magn Reson Med*. 2004; 52:115–22. [PubMed: 15236374]
- Jezzard P. Correction of geometric distortion in fMRI data. *Neuroimage*. 2012; 62:648–51. [PubMed: 21945795]
- Jiang J, Wu Y, Huang M, Yang W, Chen W, Feng Q. 3D brain tumor segmentation in multimodal MR images based on learning population- and patient-specific feature sets. *Comput Med Imaging Graph*. 2013; 37:512–21. [PubMed: 23816459]
- Johansson A, Garpebring A, Asklund T, Nyholm T. CT substitutes derived from MR images reconstructed with parallel imaging. *Med Phys*. 2014; 41:082302.
- Johansson A, Karlsson M, Nyholm T. CT substitute derived from MRI sequences with ultrashort echo time. *Med Phys*. 2011; 38:2708–14. [PubMed: 21776807]
- Jolicoeur M, Racine ML, Trop I, Hathout L, Nguyen D, Derashodian T, David S. Localization of the surgical bed using supine magnetic resonance and computed tomography scan fusion for planification of breast interstitial brachytherapy. *Radiother Oncol*. 2011; 100:480–4. [PubMed: 21924509]
- Jones, D., editor. *Diffusion MRI Theory, Methods and Applications*. OUP; USA: 2011.

- Jonsson JH, Garpebring A, Karlsson MG, Nyholm T. Internal fiducial markers and susceptibility effects in MRI-simulation and measurement of spatial accuracy. *Int J Radiat Oncol Biol Phys.* 2012; 82:1612–8. [PubMed: 21477942]
- Jonsson JH, Johansson A, Soderstrom K, Asklund T, Nyholm T. Treatment planning of intracranial targets on MRI derived substitute CT data. *Radiother Oncol.* 2013; 108:118–22. [PubMed: 23830190]
- Jovicich J, Czanner S, Greve D, Haley E, van der Kouwe A, Gollub R, Kennedy D, Schmitt F, Brown G, Macfall J, Fischl B, et al. Reliability in multi-site structural MRI studies: effects of gradient non-linearity correction on phantom and human data. *Neuroimage.* 2006; 30:436–43. [PubMed: 16300968]
- Kapanen M, Collan J, Beule A, Seppala T, Saarihahti K, Tenhunen M. Commissioning of MRI-only based treatment planning procedure for external beam radiotherapy of prostate. *Magn Reson Med.* 2013; 70:127–35. [PubMed: 22886780]
- Kapanen M, Tenhunen M. T1/T2*-weighted MRI provides clinically relevant pseudo-CT density data for the pelvic bones in MRI-only based radiotherapy treatment planning. *Acta Oncol.* 2013; 52:612–8. [PubMed: 22712634]
- Karotki A, Mah K, Meijer G, Meltsner M. Comparison of bulk electron density and voxel-based electron density treatment planning. *J Appl Clin Med Phys.* 2011; 12:3522. [PubMed: 22089006]
- Katayama N, Takemoto M, Yoshio K, Katsui K, Uesugi T, Nasu Y, Matsushita T, Kaji M, Kumon H, Kanazawa S. T2*-weighted image/T2-weighted image fusion in postimplant dosimetry of prostate brachytherapy. *J Radiat Res.* 2011; 52:680–4. [PubMed: 21857148]
- Kaza E, Symonds-Taylor R, Collins DJ, McDonald F, Mcnair HA, Scurr ED, Koh DM, Leach MO. First MRI application of an active breathing coordinator. *Phys Med Biol.* 2015 Accepted.
- Kennan, RP.; Jager, HR. T2 and T2*-w DCE-MRI: Blood perfusion and volume estimation using bolus tracking. *Quantitative MRI of the Brain.* Tofts, PS., editor. John Wiley; 2003.
- Khoo VS, Dearnaley DP, Finnigan DJ, Padhani A, Tanner SF, Leach MO. Magnetic resonance imaging (MRI): considerations and applications in radiotherapy treatment planning. *Radiother Oncol.* 1997; 42:1–15. [PubMed: 9132820]
- Kim Y, Hsu IC, Lessard E, Kurhanewicz J, Noworolski SM, Pouliot J. Class solution in inverse planned HDR prostate brachytherapy for dose escalation of DIL defined by combined MRI/MRSI. *Radiother Oncol.* 2008; 88:148–55. [PubMed: 18083260]
- Kim YJ, Kim JY, Kim TH, Lim YK, Yoon MG, Joo JN, Park SY. Dosimetric evaluation of magnetic resonance imaging-based intracavitary brachytherapy for cervical cancer. *Technol Cancer Res Treat.* 2014; 13:243–51. [PubMed: 23919398]
- Kincses ZT, Szabo N, Valalik I, Kopniczky Z, Dezi L, Klivenyi P, Jenkinson M, Kiraly A, Babos M, Voros E, Barzo P, et al. Target identification for stereotactic thalamotomy using diffusion tractography. *PLoS One.* 2012; 7:e29969. [PubMed: 22238685]
- Koch KM, Brau AC, Chen W, Gold GE, Hargreaves BA, Koff M, McKinnon GC, Potter HG, King KF. Imaging near metal with a MAVRIC-SEMAC hybrid. *Magn Reson Med.* 2011; 65:71–82. [PubMed: 20981709]
- Koch KM, Lorbiecki JE, Hinks RS, King KF. A multispectral three-dimensional acquisition technique for imaging near metal implants. *Magn Reson Med.* 2009; 61:381–90. [PubMed: 19165901]
- Koch N, Liu HH, Starkschall G, Jacobson M, Forster K, Liao Z, Komaki R, Stevens CW. Evaluation of internal lung motion for respiratory-gated radiotherapy using MRI: Part I--correlating internal lung motion with skin fiducial motion. *Int J Radiat Oncol Biol Phys.* 2004; 60:1459–72. [PubMed: 15590177]
- Koga T, Maruyama K, Kamada K, Ota T, Shin M, Itoh D, Kunii N, Ino K, Terahara A, Aoki S, Masutani Y, et al. Outcomes of diffusion tensor tractography-integrated stereotactic radiosurgery. *Int J Radiat Oncol Biol Phys.* 2012; 82:799–802. [PubMed: 21277103]
- Koh DM, Brown G, Collins DJ. Nanoparticles in rectal cancer imaging. *Cancer Biomark.* 2009; 5:89–98. [PubMed: 19414926]
- Korsholm ME, Waring LW, Edmund JM. A criterion for the reliable use of MRI-only radiotherapy. *Radiat Oncol.* 2014; 9:16. [PubMed: 24405515]

- Kovacs A, Toth L, Glavak C, Lakosi F, Hadjiev J, Bajzik G, Vandulek C, Repa I. Integrating functional MRI information into radiotherapy planning of CNS tumors-early experiences. *Pathol Oncol Res.* 2011; 17:207–17. [PubMed: 20848253]
- Legendijk JJ, Raaymakers BW, Raaijmakers AJ, Overweg J, Brown KJ, Kerkhof EM, van der Put RW, Hardemark B, van Vulpen M, van der Heide UA. MRI/linac integration. *Radiother Oncol.* 2008; 86:25–9. [PubMed: 18023488]
- Legendijk, JJ.; Raaymakers, BW.; ven den Berg, C.; Moerland, M.; Philippens, ME.; van Vulpen, M. 2014. (MRI linacs; review submitted to PMB 2014)
- Lambert J, Greer PB, Menk F, Patterson J, Parker J, Dahl K, Gupta S, Capp A, Wratten C, Tang C, Kumar M, et al. MRI-guided prostate radiation therapy planning: Investigation of dosimetric accuracy of MRI-based dose planning. *Radiother Oncol.* 2011; 98:330–4. [PubMed: 21339009]
- Lee YK, Bollet M, Charles-Edwards G, Flower MA, Leach MO, McNair H, Moore E, Rowbottom C, Webb S. Radiotherapy treatment planning of prostate cancer using magnetic resonance imaging alone. *Radiother Oncol.* 2003; 66:203–16. [PubMed: 12648793]
- Li XA, Wang JZ, Jursinic PA, Lawton CA, Wang D. Dosimetric advantages of IMRT simultaneous integrated boost for high-risk prostate cancer. *Int J Radiat Oncol Biol Phys.* 2005; 61:1251–7. [PubMed: 15752907]
- Liu HH, Koch N, Starkschall G, Jacobson M, Forster K, Liao Z, Komaki R, Stevens CW. Evaluation of internal lung motion for respiratory-gated radiotherapy using MRI: Part II-margin reduction of internal target volume. *Int J Radiat Oncol Biol Phys.* 2004; 60:1473–83. [PubMed: 15590178]
- Lu W, Pauly KB, Gold GE, Pauly JM, Hargreaves BA. SEMAC: Slice Encoding for Metal Artifact Correction in MRI. *Magn Reson Med.* 2009; 62:66–76. [PubMed: 19267347]
- Maikusa N, Yamashita F, Tanaka K, Abe O, Kawaguchi A, Kabasawa H, Chiba S, Kasahara A, Kobayashi N, Yuasa T, Sato N, et al. Improved volumetric measurement of brain structure with a distortion correction procedure using an ADNI phantom. *Med Phys.* 2013; 40:062303. [PubMed: 23718605]
- Martinez-Moller A, Nekolla SG. Attenuation correction for PET/MR: problems, novel approaches and practical solutions. *Z Med Phys.* 2012; 22:299–310. [PubMed: 22925653]
- Marx M, Ehrhardt J, Werner R, Schlemmer HP, Handels H. Simulation of spatiotemporal CT data sets using a 4D MRI-based lung motion model. *Int J Comput Assist Radiol Surg.* 2014; 9:401–9. [PubMed: 24323401]
- Mast M, Coerkamp E, Heijenbrok M, Scholten A, Jansen W, Kouwenhoven E, Nijkamp J, de Waard S, Petoukhova A, Struikmans H. Target volume delineation in breast conserving radiotherapy: are co-registered CT and MR images of added value. *Radiat Oncol.* 2014; 9:65. [PubMed: 24571843]
- Mcrobbie, DW.; Moore, EA.; Graves, MJ.; Prince, MR. MRI: From Picture to Proton. Cambridge, UK: Cambridge University Press; 2003.
- Minniti G, Amelio D, Amichetti M, Salvati M, Muni R, Bozzao A, Lanzetta G, Scarpino S, Arcella A, Enrici RM. Patterns of failure and comparison of different target volume delineations in patients with glioblastoma treated with conformal radiotherapy plus concomitant and adjuvant temozolomide. *Radiother Oncol.* 2010; 97:377–81. [PubMed: 20855119]
- Mizowaki T, Nagata Y, Okajima K, Kokubo M, Negoro Y, Araki N, Hiraoka M. Reproducibility of geometric distortion in magnetic resonance imaging based on phantom studies. *Radiother Oncol.* 2000; 57:237–42. [PubMed: 11054528]
- Mueller-Lisse UG, Swanson MG, Vigneron DB, Kurhanewicz J. Magnetic resonance spectroscopy in patients with locally confined prostate cancer: association of prostatic citrate and metabolic atrophy with time on hormone deprivation therapy, PSA level, and biopsy Gleason score. *Eur Radiol.* 2007; 17:371–8. [PubMed: 16791635]
- Nelson SJ, Graves E, Pirzkall A, Li X, Antiniw Chan A, Vigneron DB, Mcknight TR. In vivo molecular imaging for planning radiation therapy of gliomas: an application of 1H MRSI. *J Magn Reson Imaging.* 2002; 16:464–76. [PubMed: 12353260]
- Nelson SJ, Kurhanewicz J, Vigneron DB, Larson PE, Harzstark AL, Ferrone M, van Criekinge M, Chang JW, Bok R, Park I, Reed G, et al. Metabolic imaging of patients with prostate cancer using hyperpolarized [1-(1)3C]pyruvate. *Sci Transl Med.* 2013; 5:198ra108.

- Newbold K, Partridge M, Cook G, Sohaib SA, Charles-Edwards E, Rhys-Evans P, Harrington K, Nutting C. Advanced imaging applied to radiotherapy planning in head and neck cancer: a clinical review. *Br J Radiol.* 2006; 79:554–61. [PubMed: 16823059]
- Nichol AM, Brock KK, Lockwood GA, Moseley DJ, Rosewall T, Warde PR, Catton CN, Jaffray DA. A magnetic resonance imaging study of prostate deformation relative to implanted gold fiducial markers. *Int J Radiat Oncol Biol Phys.* 2007; 67:48–56. [PubMed: 17084546]
- Nishiyama T, Tomita Y, Takahashi K. Influence of androgen deprivation therapy on volume of anatomic zones of prostate in patients with prostate cancer using magnetic resonance imaging. *Urology.* 2004; 63:917–21. [PubMed: 15134981]
- Nutting CM, Corbishley CM, Sanchez-Nieto B, Cosgrove VP, Webb S, Dearnaley DP. Potential improvements in the therapeutic ratio of prostate cancer irradiation: dose escalation of pathologically identified tumour nodules using intensity modulated radiotherapy. *Br J Radiol.* 2002; 75:151–61. [PubMed: 11893639]
- Nuyts S. Defining the target for radiotherapy of head and neck cancer. *Cancer Imaging.* 2007; 7(Spec No A):S50–5. [PubMed: 17921086]
- O'Neill BD, Salerno G, Thomas K, Tait DM, Brown G. MR vs CT imaging: low rectal cancer tumour delineation for three-dimensional conformal radiotherapy. *Br J Radiol.* 2009; 82:509–13. [PubMed: 19153180]
- Ohashi T, Momma T, Yamashita S, Nagatsuma K, Kanai K, Kitagawa K, Takahashi S, Hanada T, Yorozu A, Shigematsu N. Impact of MRI-based postimplant dosimetric assessment in prostate brachytherapy using contrast-enhanced T1-weighted images. *Brachytherapy.* 2012; 11:468–75. [PubMed: 22330102]
- Onal C, Sonmez S, Erbay G, Guler OC, Arslan G. Simultaneous integrated boost to intraprostatic lesions using different energy levels of intensity-modulated radiotherapy and volumetric-arc therapy. *Br J Radiol.* 2014; 87:20130617. [PubMed: 24319009]
- Padhani AR, Liu G, Koh DM, Chenevert TL, Thoeny HC, Takahara T, Dzik-Jurasz A, Ross BD, van Cauteren M, Collins D, Hammoud DA, et al. Diffusion-weighted magnetic resonance imaging as a cancer biomarker: consensus and recommendations. *Neoplasia.* 2009; 11:102–25. [PubMed: 19186405]
- Padhani AR, Macvicar AD, Gapinski CJ, Dearnaley DP, Parker GJ, Suckling J, Leach MO, Husband JE. Effects of androgen deprivation on prostatic morphology and vascular permeability evaluated with mr imaging. *Radiology.* 2001; 218:365–74. [PubMed: 11161148]
- Panek R, Scurr E, Bernard J, Revell P, Koh D, Hansen V, Saran F, Leach M, Schmidt M. SEMAC MRI Metal Artifact Reduction Technique for Radiotherapy Planning Using CT/MRI Fusio. *Medical Physics.* 2013; 40:175.
- Pantelis E, Papadakis N, Verigos K, Stathochristopoulou I, Antypas C, Lekas L, Tzouras A, Georgiou E, Salvaras N. Integration of functional MRI and white matter tractography in stereotactic radiosurgery clinical practice. *Int J Radiat Oncol Biol Phys.* 2010; 78:257–67. [PubMed: 20421146]
- Parker CC, Damyanovich A, Haycocks T, Haider M, Bayley A, Catton CN. Magnetic resonance imaging in the radiation treatment planning of localized prostate cancer using intra-prostatic fiducial markers for computed tomography co-registration. *Radiother Oncol.* 2003; 66:217–24. [PubMed: 12648794]
- Partovi S, Robbin MR, Steinbach OC, Kohan A, Rubbert C, Vercher-Conejero JL, Kolthammer JA, Faulhaber P, Paspulati RM, Ros PR. Initial experience of MR/PET in a clinical cancer center. *J Magn Reson Imaging.* 2014; 39:768–80. [PubMed: 24006287]
- Partridge M, Yamamoto T, Grau C, Hoyer M, Muren LP. Imaging of normal lung, liver and parotid gland function for radiotherapy. *Acta Oncol.* 2010; 49:997–1011. [PubMed: 20831488]
- Pech M, Mohnike K, Wieners G, Bialek E, Dudeck O, Seidensticker M, Peters N, Wust P, Gademann G, Ricke J. Radiotherapy of liver metastases. Comparison of target volumes and dose-volume histograms employing CT- or MRI-based treatment planning. *Strahlenther Onkol.* 2008; 184:256–61. [PubMed: 18427756]
- Peet AC, Arvanitis TN, Leach MO, Waldman AD. Functional imaging in adult and paediatric brain tumours. *Nat Rev Clin Oncol.* 2012; 9:700–11. [PubMed: 23149894]

- Pirzkall A, MCGue C, Saraswathy S, Cha S, Liu R, Vandenberg S, Lamborn KR, Berger MS, Chang SM, Nelson SJ. Tumor regrowth between surgery and initiation of adjuvant therapy in patients with newly diagnosed glioblastoma. *Neuro Oncol.* 2009; 11:842–52. [PubMed: 19229057]
- Plathow C, Fink C, Ley S, Puderbach M, Eichinger M, Zuna I, Schmahl A, Kauczor HU. Measurement of tumor diameter-dependent mobility of lung tumors by dynamic MRI. *Radiother Oncol.* 2004a; 73:349–54. [PubMed: 15588881]
- Plathow C, Ley S, Fink C, Puderbach M, Hosch W, Schmahl A, Debus J, Kauczor HU. Analysis of intrathoracic tumor mobility during whole breathing cycle by dynamic MRI. *Int J Radiat Oncol Biol Phys.* 2004b; 59:952–9. [PubMed: 15234028]
- Plewes DB, Kucharczyk W. Physics of MRI: a primer. *J Magn Reson Imaging.* 2012; 35:1038–54. [PubMed: 22499279]
- Potter R, Haie-Meder C, Van Limbergen E, Barillot I, De Brabandere M, Dimopoulos J, Dumas I, Erickson B, Lang S, Nulens A, Petrow P, et al. Recommendations from gynaecological (GYN) GEC ESTRO working group (II): concepts and terms in 3D image-based treatment planning in cervix cancer brachytherapy-3D dose volume parameters and aspects of 3D image-based anatomy, radiation physics, radiobiology. *Radiother Oncol.* 2006; 78:67–77. [PubMed: 16403584]
- Pouliot J, Kim Y, Lessard E, Hsu IC, Vigneron DB, Kurhanewicz J. Inverse planning for HDR prostate brachytherapy used to boost dominant intraprostatic lesions defined by magnetic resonance spectroscopy imaging. *Int J Radiat Oncol Biol Phys.* 2004; 59:1196–207. [PubMed: 15234056]
- Powell C, Schmidt M, Borri M, Koh DM, Partridge M, Riddell A, Cook G, Bhide SA, Nutting CM, Harrington KJ, Newbold KL. Changes in functional imaging parameters following induction chemotherapy have important implications for individualised patient-based treatment regimens for advanced head and neck cancer. *Radiother Oncol.* 2013; 106:112–7. [PubMed: 23089306]
- Pu AT, Sandler HM, Radany EH, Blaivas M, Page MA, Greenberg HS, Junck L, Ross DA. Low grade gliomas: preliminary analysis of failure patterns among patients treated using 3D conformal external beam irradiation. *Int J Radiat Oncol Biol Phys.* 1995; 31:461–6. [PubMed: 7852107]
- Quon H, Brizel DM. Predictive and prognostic role of functional imaging of head and neck squamous cell carcinomas. *Semin Radiat Oncol.* 2012; 22:220–32. [PubMed: 22687947]
- Radawski JD, Huang Z, Wang JZ, Yuh WT, Mayr NA. Direct sagittal image registration and tumor delineation on sagittal magnetic resonance imaging sequences for image-guided brachytherapy of cervical cancer. *Discov Med.* 2012; 13:47–56. [PubMed: 22284783]
- Rahbar H, Partridge SC, Demartini WB, Thursten B, Lehman CD. Clinical and technical considerations for high quality breast MRI at 3 Tesla. *J Magn Reson Imaging.* 2013; 37:778–90. [PubMed: 23526757]
- Rasch C, Barillot I, Remeijer P, Touw A, van Herk M, Lebesque JV. Definition of the prostate in CT and MRI: a multi-observer study. *Int J Radiat Oncol Biol Phys.* 1999; 43:57–66. [PubMed: 9989514]
- Reinsberg SA, Doran SJ, Charles-Edwards EM, Leach MO. A complete distortion correction for MR images: II. Rectification of static-field inhomogeneities by similarity-based profile mapping. *Phys Med Biol.* 2005; 50:2651–61. [PubMed: 15901960]
- Riches SF, Partridge M, Payne GS, Morgan VA, Desouza NM. Scaling methods to account for shrinkage of the prostate during androgen ablation for registration of tumor position between pre- and post-treatment MR images. *International Society for Magnetic Resonance in Medicine, 17th Annual Meeting; 2009a.* p. 2908
- Riches SF, Payne GS, Desouza NM, Dearnaley D, Morgan VA, Morgan SC, Partridge M. Effect on therapeutic ratio of planning a boosted radiotherapy dose to the dominant intraprostatic tumour lesion within the prostate based on multifunctional MR parameters. *Br J Radiol.* 2014:20130813. [PubMed: 24601648]
- Riches SF, Payne GS, Morgan VA, Sandhu S, Fisher C, Germuska M, Collins DJ, Thompson A, Desouza NM. MRI in the detection of prostate cancer: combined apparent diffusion coefficient, metabolite ratio, and vascular parameters. *AJR Am J Roentgenol.* 2009b; 193:1583–91. [PubMed: 19933651]

- Ricke J, Thormann M, Ludewig M, Jungnickel K, Grosser O, Wybranski C, Peters N, Hass P, Bunke J, Fischbach F. MR-guided liver tumor ablation employing open high-field 1.0T MRI for image-guided brachytherapy. *Eur Radiol*. 2010; 20:1985–93. [PubMed: 20306080]
- Robson MD, Gatehouse PD, Bydder M, Bydder GM. Magnetic resonance: an introduction to ultrashort TE (UTE) imaging. *J Comput Assist Tomogr*. 2003; 27:825–46. [PubMed: 14600447]
- Roels S, Slagmolen P, Nuyts J, Lee JA, Loeckx D, Maes F, Vandecaveye V, Stroobants S, Ectors N, Penninckx F, Haustermans K. Biological image-guided radiotherapy in rectal cancer: challenges and pitfalls. *Int J Radiat Oncol Biol Phys*. 2009; 75:782–90. [PubMed: 19289265]
- Sander L, Langkilde NC, Holmberg M, Carl J. MRI target delineation may reduce long-term toxicity after prostate radiotherapy. *Acta Oncol*. 2013
- Schmitz AC, van den Bosch MA, Loo CE, Mali WP, Bartelink H, Gertenbach M, Holland R, Peterse JL, Rutgers EJ, Gilhuijs KG. Precise correlation between MRI and histopathology - exploring treatment margins for MRI-guided localized breast cancer therapy. *Radiother Oncol*. 2010; 97:225–32. [PubMed: 20826026]
- Seevinck PR, de Leeuw H, Bos C, Bakker CJ. Highly localized positive contrast of small paramagnetic objects using 3D center-out radial sampling with off-resonance reception. *Magn Reson Med*. 2011; 65:146–56. [PubMed: 20740656]
- Seppenwoolde Y, Shirato H, Kitamura K, Shimizu S, van Herk M, Lebesque JV, Miyasaka K. Precise and real-time measurement of 3D tumor motion in lung due to breathing and heartbeat, measured during radiotherapy. *Int J Radiat Oncol Biol Phys*. 2002; 53:822–34. [PubMed: 12095547]
- Shihab OC, Moran BJ, Heald RJ, Quirke P, Brown G. MRI staging of low rectal cancer. *Eur Radiol*. 2009; 19:643–50. [PubMed: 18810451]
- Singh AK, Guion P, Sears-Crouse N, Ullman K, Smith S, Albert PS, Fichtinger G, Choyke PL, Xu S, Kruecker J, Wood BJ, et al. Simultaneous integrated boost of biopsy proven, MRI defined dominant intra-prostatic lesions to 95 Gray with IMRT: early results of a phase I NCI study. *Radiat Oncol*. 2007; 2:36. [PubMed: 17877821]
- Smith BD, Arthur DW, Buchholz TA, Haffty BG, Hahn CA, Hardenbergh PH, Julian TB, Marks LB, Todor DA, Vicini FA, Whelan TJ, et al. Accelerated partial breast irradiation consensus statement from the American Society for Radiation Oncology (ASTRO). *Int J Radiat Oncol Biol Phys*. 2009; 74:987–1001. [PubMed: 19545784]
- Stadlbauer A, Ganslandt O, Buslei R, Hammen T, Gruber S, Moser E, Buchfelder M, Salomonowitz E, Nimsky C. Gliomas: histopathologic evaluation of changes in directionality and magnitude of water diffusion at diffusion-tensor MR imaging. *Radiology*. 2006; 240:803–10. [PubMed: 16926329]
- Stall B, Zach L, Ning H, Ondos J, Arora B, Shankavaram U, Miller RW, Citrin D, Camphausen K. Comparison of T2 and FLAIR imaging for target delineation in high grade gliomas. *Radiat Oncol*. 2010; 5:5. [PubMed: 20109218]
- Stejskal EO, Tanner JE. Spin diffusion measurements: Spin echoes in the presence of a time-dependent field gradient. *Journal of Chemical Physics*. 1965; 42:288–292.
- Tamada T, Sone T, Jo Y, Toshimitsu S, Yamashita T, Yamamoto A, Tanimoto D, Ito K. Apparent diffusion coefficient values in peripheral and transition zones of the prostate: comparison between normal and malignant prostatic tissues and correlation with histologic grade. *J Magn Reson Imaging*. 2008; 28:720–6. [PubMed: 18777532]
- Tan J, Lim Joon D, Fitt G, Wada M, Lim Joon M, Mercuri A, Marr M, Chao M, Khoo V. The utility of multimodality imaging with CT and MRI in defining rectal tumour volumes for radiotherapy treatment planning: a pilot study. *J Med Imaging Radiat Oncol*. 2010; 54:562–8. [PubMed: 21199435]
- Tan LT. Implementation of image-guided brachytherapy for cervix cancer in the UK: progress update. *Clin Oncol (R Coll Radiol)*. 2011; 23:681–4. [PubMed: 21843928]
- Tanimoto A, Kuribayashi S. Application of superparamagnetic iron oxide to imaging of hepatocellular carcinoma. *Eur J Radiol*. 2006; 58:200–16. [PubMed: 16414230]
- Tavares WM, Tustumi F, da Costa Leite C, Fernel Gamarra L, Amaro E Jr, Teixeira MJ, Fonoff ET. An image correction protocol to reduce distortion for 3-T stereotactic MRI. *Neurosurgery*. 2014; 74:121–6. discussion126-7. [PubMed: 24064479]

- Taylor A, Powell ME. An assessment of interfractional uterine and cervical motion: implications for radiotherapy target volume definition in gynaecological cancer. *Radiother Oncol*. 2008; 88:250–7. [PubMed: 18538873]
- Thariat J, Castelli J, Chanalet S, Marcie S, Mammar H, Bondiau PY. CyberKnife stereotactic radiotherapy for spinal tumors: value of computed tomographic myelography in spinal cord delineation. *Neurosurgery*. 2009; 64:A60–6. [PubMed: 19165075]
- Tofts PS, Kermode AG. Measurement of the blood-brain barrier permeability and leakage space using dynamic MR imaging. 1. Fundamental concepts. *Magn Reson Med*. 1991; 17:357–67. [PubMed: 2062210]
- Topolnjak R, Borst GR, Nijkamp J, Sonke JJ. Image-guided radiotherapy for left-sided breast cancer patients: geometrical uncertainty of the heart. *Int J Radiat Oncol Biol Phys*. 2012; 82:e647–55. [PubMed: 22270162]
- Uh J, Merchant TE, Li Y, Li X, Hua C. MRI-based treatment planning with pseudo CT generated through atlas registration. *Med Phys*. 2014; 41:051711. [PubMed: 24784377]
- Ulin K, Urie MM, Cherlow JM. Results of a multi-institutional benchmark test for cranial CT/MR image registration. *Int J Radiat Oncol Biol Phys*. 2010; 77:1584–9. [PubMed: 20381270]
- van den Bergh RC, Ahmed HU, Bangma CH, Cooperberg MR, Villers A, Parker CC. Novel Tools to Improve Patient Selection and Monitoring on Active Surveillance for Low-risk Prostate Cancer: A Systematic Review. *Eur Urol*. 2014
- van der Heide UA, Kotte AN, Dehnad H, Hofman P, Lagenijk JJ, van Vulpen M. Analysis of fiducial marker-based position verification in the external beam radiotherapy of patients with prostate cancer. *Radiother Oncol*. 2007; 82:38–45. [PubMed: 17141903]
- vandecaveye V, de Keyzer F, Nuyts S, Deraedt K, Dirix P, Hamaekers P, Vander Poorten V, Delaere P, Hermans R. Detection of head and neck squamous cell carcinoma with diffusion weighted MRI after (chemo)radiotherapy: correlation between radiologic and histopathologic findings. *Int J Radiat Oncol Biol Phys*. 2007; 67:960–71. [PubMed: 17141979]
- Vargas MI, Becker M, Garibotto V, Heinzer S, Loubeyre P, Gariani J, Lovblad K, Vallee JP, Ratib O. Approaches for the optimization of MR protocols in clinical hybrid PET/MRI studies. *MAGMA*. 2013; 26:57–69. [PubMed: 23008016]
- Varma G, Clough RE, Acher P, Senegas J, Dahnke H, Keevil SF, Schaeffter T. Positive visualization of implanted devices with susceptibility gradient mapping using the original resolution. *Magn Reson Med*. 2011; 65:1483–90. [PubMed: 21500272]
- Verma S, Turkbey B, Muradyan N, Rajesh A, Cornud F, Haider MA, Choyke PL, Harisinghani M. Overview of dynamic contrast-enhanced MRI in prostate cancer diagnosis and management. *AJR Am J Roentgenol*. 2012; 198:1277–88. [PubMed: 22623539]
- Viswanathan AN, Dimopoulos J, Kirisits C, Berger D, Potter R. Computed tomography versus magnetic resonance imaging-based contouring in cervical cancer brachytherapy: results of a prospective trial and preliminary guidelines for standardized contours. *Int J Radiat Oncol Biol Phys*. 2007; 68:491–8. [PubMed: 17331668]
- Vonken EJ, Schar M, Yu J, Bakker CJ, Stuber M. Direct in vitro comparison of six three-dimensional positive contrast methods for susceptibility marker imaging. *J Magn Reson Imaging*. 2013; 38:344–57. [PubMed: 23281151]
- Voroney JP, Brock KK, Eccles C, Haider M, Dawson LA. Prospective comparison of computed tomography and magnetic resonance imaging for liver cancer delineation using deformable image registration. *Int J Radiat Oncol Biol Phys*. 2006; 66:780–91. [PubMed: 17011453]
- Wanderas AD, Sundset M, Langdal I, Danielsen S, Frykholm G, Marthinsen AB. Adaptive brachytherapy of cervical cancer, comparison of conventional point A and CT based individual treatment planning. *Acta Oncol*. 2012; 51:345–54. [PubMed: 22035118]
- Wang D, Doddrell DM. Geometric distortion in structural magnetic resonance imaging. *Current Medical Imaging Reviews*. 2005; 1:49–60.
- Wang D, Doddrell DM, Cowin G. A novel phantom and method for comprehensive 3-dimensional measurement and correction of geometric distortion in magnetic resonance imaging. *Magn Reson Imaging*. 2004a; 22:529–42. [PubMed: 15120173]

- Wang D, Strugnell W, Cowin G, Doddrell DM, Slaughter R. Geometric distortion in clinical MRI systems Part II: correction using a 3D phantom. *Magn Reson Imaging*. 2004b; 22:1223–32. [PubMed: 15607093]
- Wang H, Balter J, Cao Y. Patient-induced susceptibility effect on geometric distortion of clinical brain MRI for radiation treatment planning on a 3T scanner. *Phys Med Biol*. 2013; 58:465–77. [PubMed: 23302471]
- Wang P, Popovtzer A, Eisbruch A, Cao Y. An approach to identify, from DCE MRI, significant subvolumes of tumors related to outcomes in advanced head-and-neck cancer. *Med Phys*. 2012a; 39:5277–85. [PubMed: 22894453]
- Wang X, Pan T, Pinnix C, Zhang SX, Salehpour M, Sun TL, Gladish G, Strom EA, Perkins GH, Tereffe W, Woodward W, et al. Cardiac motion during deep-inspiration breath-hold: implications for breast cancer radiotherapy. *Int J Radiat Oncol Biol Phys*. 2012b; 82:708–14. [PubMed: 21444161]
- Weitmann HD, Potter R, Waldhausl C, Nechvile E, Kirisits C, Knocke TH. Pilot study in the treatment of endometrial carcinoma with 3D image-based high-dose-rate brachytherapy using modified Heyman packing: clinical experience and dose-volume histogram analysis. *Int J Radiat Oncol Biol Phys*. 2005; 62:468–78. [PubMed: 15890589]
- White MJ, Hawkes DJ, Melbourne A, Collins DJ, Coolens C, Hawkins M, Leach MO, Atkinson D. Motion artifact correction in free-breathing abdominal MRI using overlapping partial samples to recover image deformations. *Magn Reson Med*. 2009; 62:440–9. [PubMed: 19449437]
- Willats L, Calamante F. The 39 steps: evading error and deciphering the secrets for accurate dynamic susceptibility contrast MRI. *NMR Biomed*. 2013; 26:913–31. [PubMed: 22782914]
- Wood ML, Henkelman RM. MR image artifacts from periodic motion. *Med Phys*. 1985; 12:143–51. [PubMed: 4000069]
- Xia P, Pickett B, Vigneault E, Verhey LJ, Roach M 3rd. Forward or inversely planned segmental multileaf collimator IMRT and sequential tomotherapy to treat multiple dominant intraprostatic lesions of prostate cancer to 90 Gy. *Int J Radiat Oncol Biol Phys*. 2001; 51:244–54. [PubMed: 11516874]
- Yang C, White J, Li XA. Deformable Breast MRI and CT Registration for Radiation Treatment Planning Using B-spline With Rigidity and Feature Point Distance Regularization. *Int J Radiat Oncol Biol Phys*. 2012; 84:S111.
- Yang TJ, Tao R, Elkhuizen PH, van Vliet-Vroegindeweij C, Li G, Powell SN. Tumor bed delineation for external beam accelerated partial breast irradiation: a systematic review. *Radiother Oncol*. 2013; 108:181–9. [PubMed: 23806188]
- Yu JI, Kim JS, Park HC, Lim DH, Han YY, Lim HC, Paik SW. Evaluation of anatomical landmark position differences between respiration-gated MRI and four-dimensional CT for radiation therapy in patients with hepatocellular carcinoma. *Br J Radiol*. 2013; 86:20120221. [PubMed: 23239694]
- Zhu X, Bourland JD, Yuan Y, Zhuang T, O'Daniel J, Thongphiew D, Wu QJ, Das SK, Yoo S, Yin FF. Tradeoffs of integrating real-time tracking into IGRT for prostate cancer treatment. *Phys Med Biol*. 2009; 54:N393–401. [PubMed: 19661570]
- Zwahlen D, Jezioranski J, Chan P, Haider MA, Cho YB, Yeung I, Levin W, Manchul L, Fyles A, Milosevic M. Magnetic resonance imaging-guided intracavitary brachytherapy for cancer of the cervix. *Int J Radiat Oncol Biol Phys*. 2009; 74:1157–64. [PubMed: 19101097]

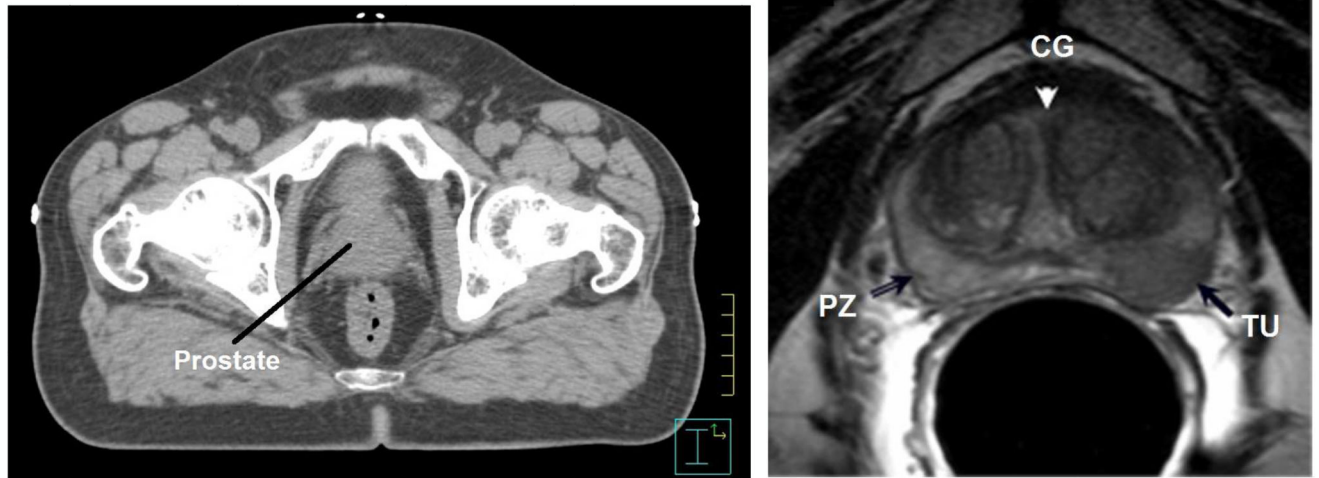
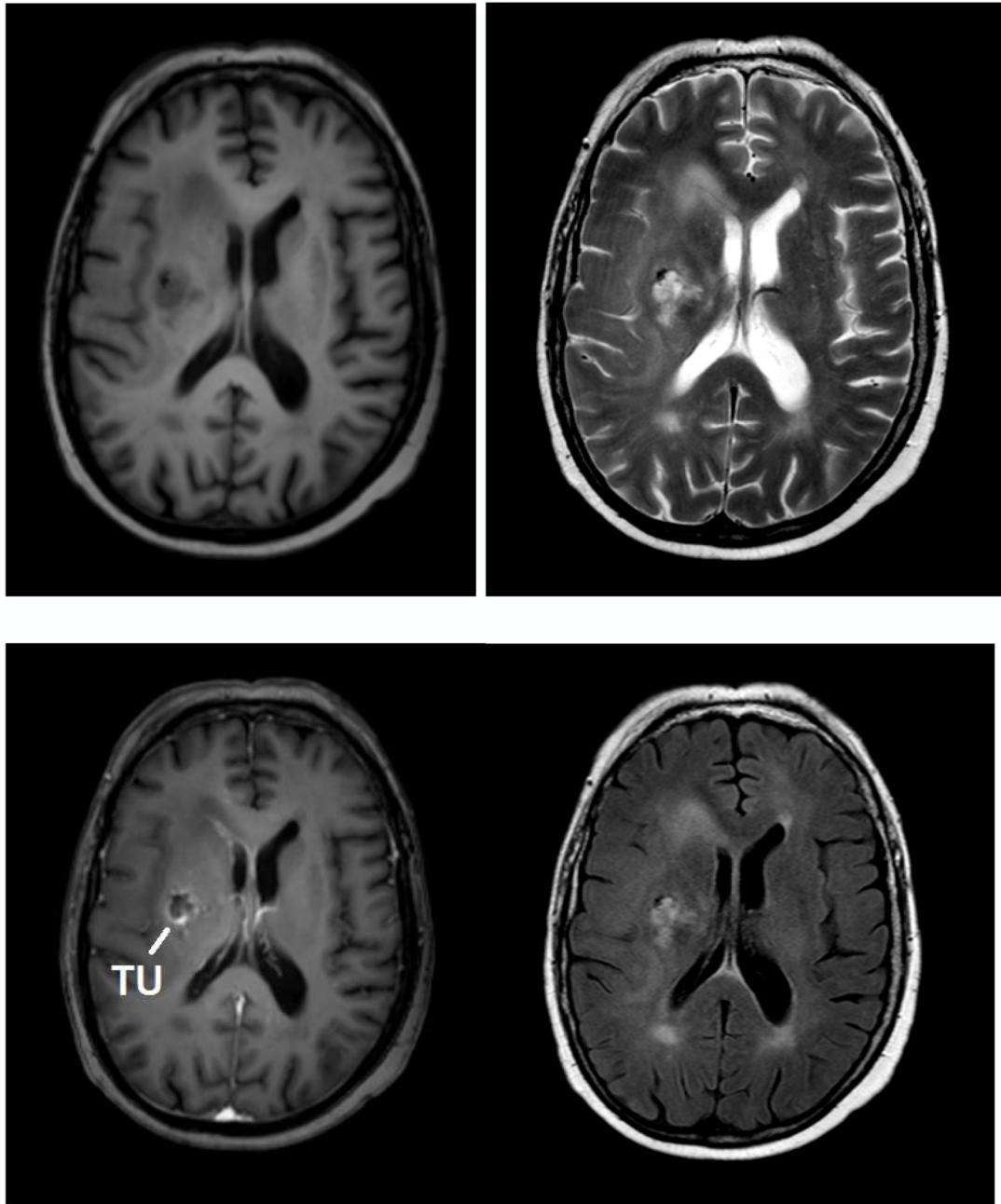


Figure 1.

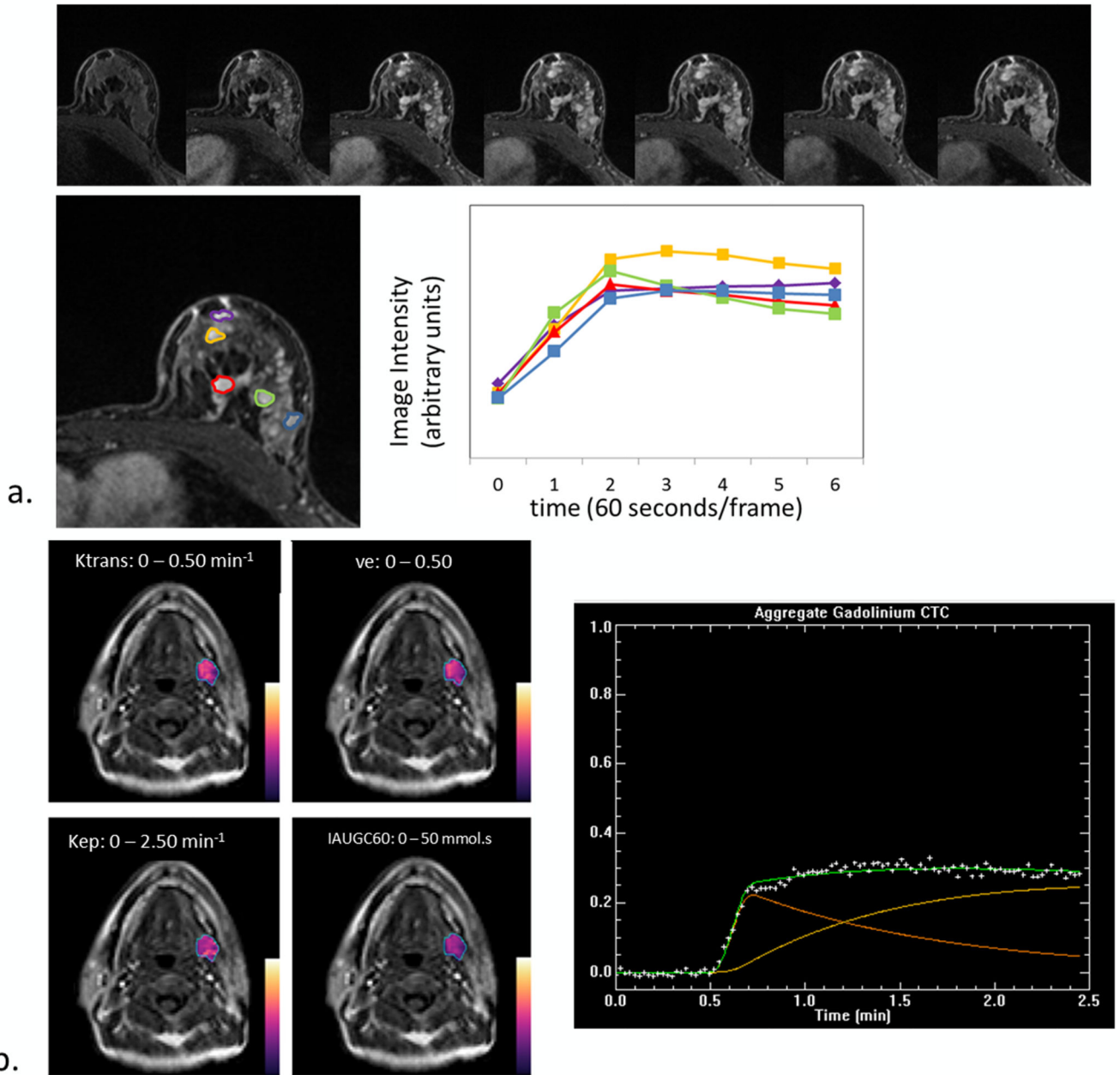
Comparison of axial CT and T2-weighted MR images to depict prostate tumours. In the CT image (left) only the boundaries of the prostate may be estimated. In the enlarged T2-weighted MR image (right) structure within the prostate is readily apparent. PZ = Peripheral Zone, CG = central gland, TU = tumour.

**Figure 2.**

Example transaxial brain images of patient with glioblastoma. Note there is no signal from cortical bone.

- a) T1-weighted image. TR/TE = 8.3ms/3.8 ms. Fluid appears darker (e.g. cerebral spinal fluid in ventricles).
- b) T2-weighted image. TR/TE = 3000/80ms. Fluid appears bright.
- c) T1-weighted images as (a) following injection of contrast agent. Note brighter signal in blood vessels, and in tumour (TU) towards left of image (patient right).

d) Fluid-attenuated inversion recovery image (FLAIR). This has a high degree of T2 weighting, but fluid is attenuated to enable other long-T2 tissues to be more conspicuous.

**Figure 3.**

a. Top. T₁-weighted transverse images through breast following administration of MRI contrast agent, acquired at 1 minute intervals. Below. The signal intensity from each of the five lesions indicated is shown for each time point. Qualitative analysis of contrast-agent uptake curves show different uptake patterns in multi-focal disease of the breast. Rapid wash in followed by a gradual wash out indicates highly vascularised lesions, most likely to be malignant. **b.** Pharmacokinetic analysis on DCE MRI of a head and neck squamous cell carcinoma. Parametric maps generated with in-house software (d'Arcy et al., 2006) are overlaid in colour showing heterogeneity within the lesion for the values of K_{trans} , v_e , K_{ep}

and IAUGC60 (Integrated area under the contrast-agent concentration curve in the first 60 seconds). Whole lesion uptake is summarised on the right.

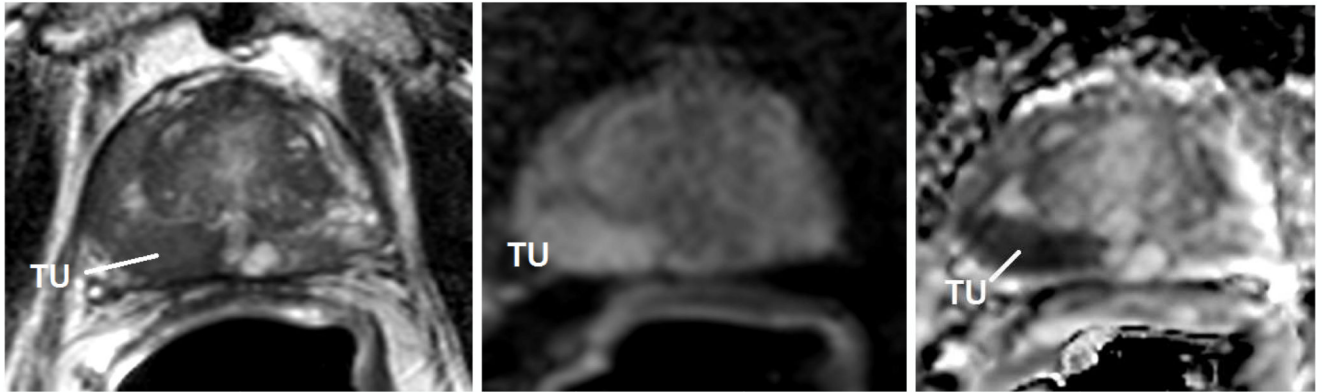


Figure 4.

Example transverse images of prostate

- a) T2-weighted image.
- b) Diffusion-weighted image. Tumour has restricted diffusion relative to normal prostate tissue and so appears bright
- c) Calculated image showing pixel-by-pixel values of calculated Apparent Diffusion Coefficient (ADC). In the ADC image the prostate lesion now appears dark.

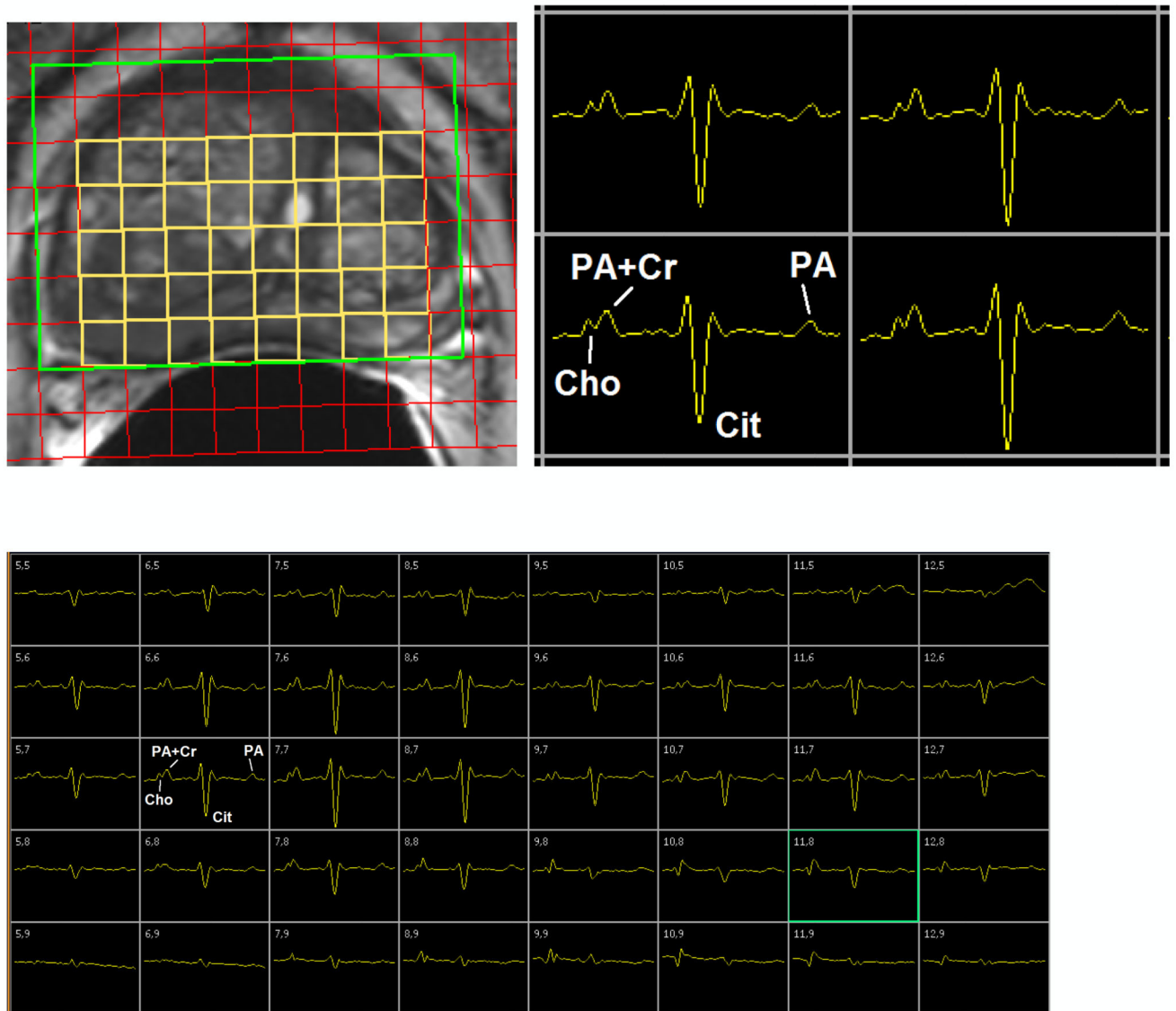


Figure 5.

Example MRSI spectra in prostate

a) MRSI grid overlying T2-w image

b) Enlarged selection from MRSI grid. Cho – choline, Cit = citrate, PA = polyamines, Cr = creatine.

c) MRSI grid over entire prostate.

Acquisition parameters: TR = 745 ms, TE = 99ms. Acquired using internal and external rf coils at 3.0T.

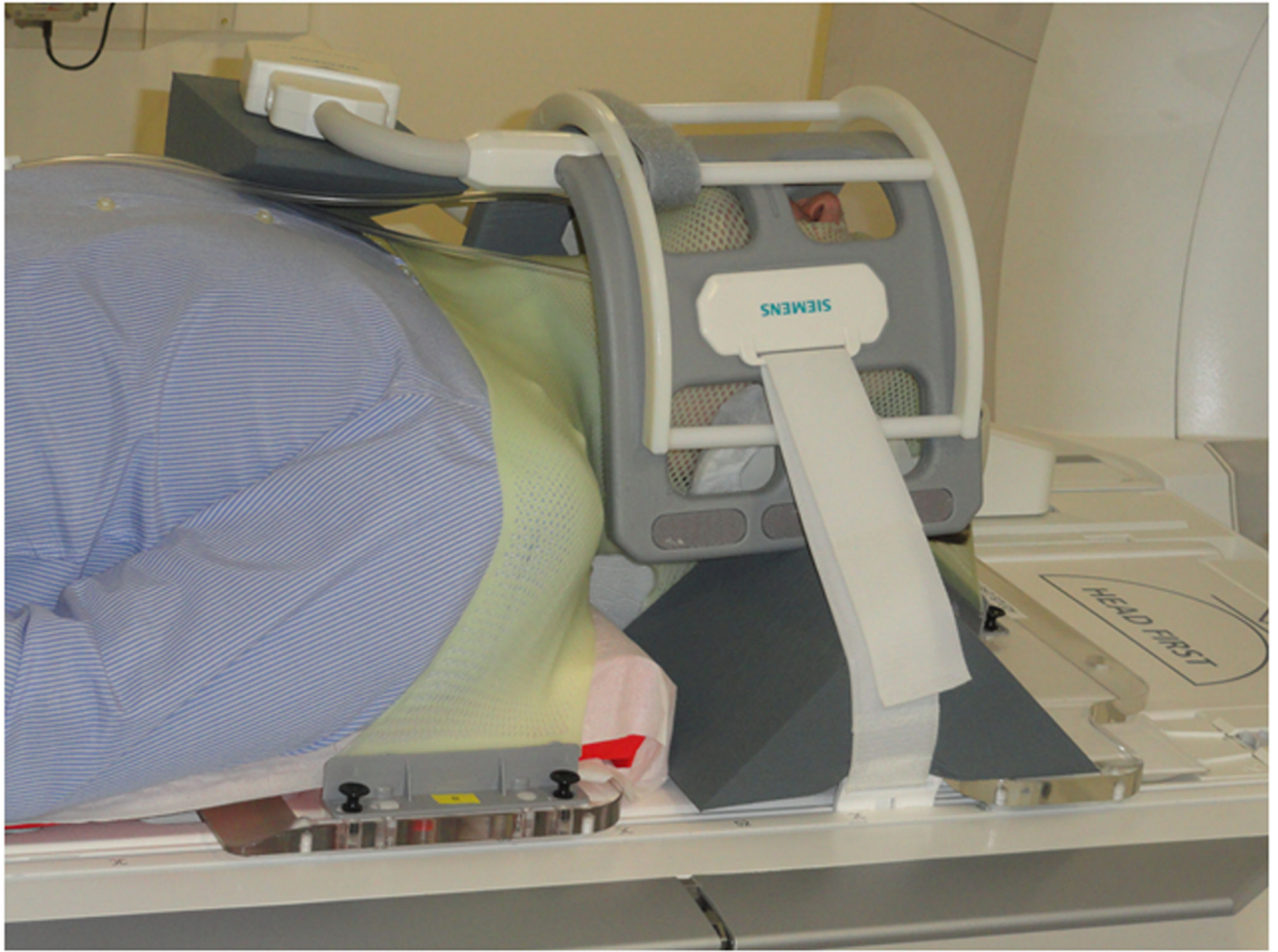


Figure 6. Receiver coil arrangement used at the Royal Marsden NHS Foundation Trust to perform Head and Neck MRI for RT planning, demonstrated on a volunteer. A standard MR-compatible baseboard is employed, enabling the use of a thermoplastic mask. The large flex-coil is positioned above the neck and used in conjunction with elements of the spine array.

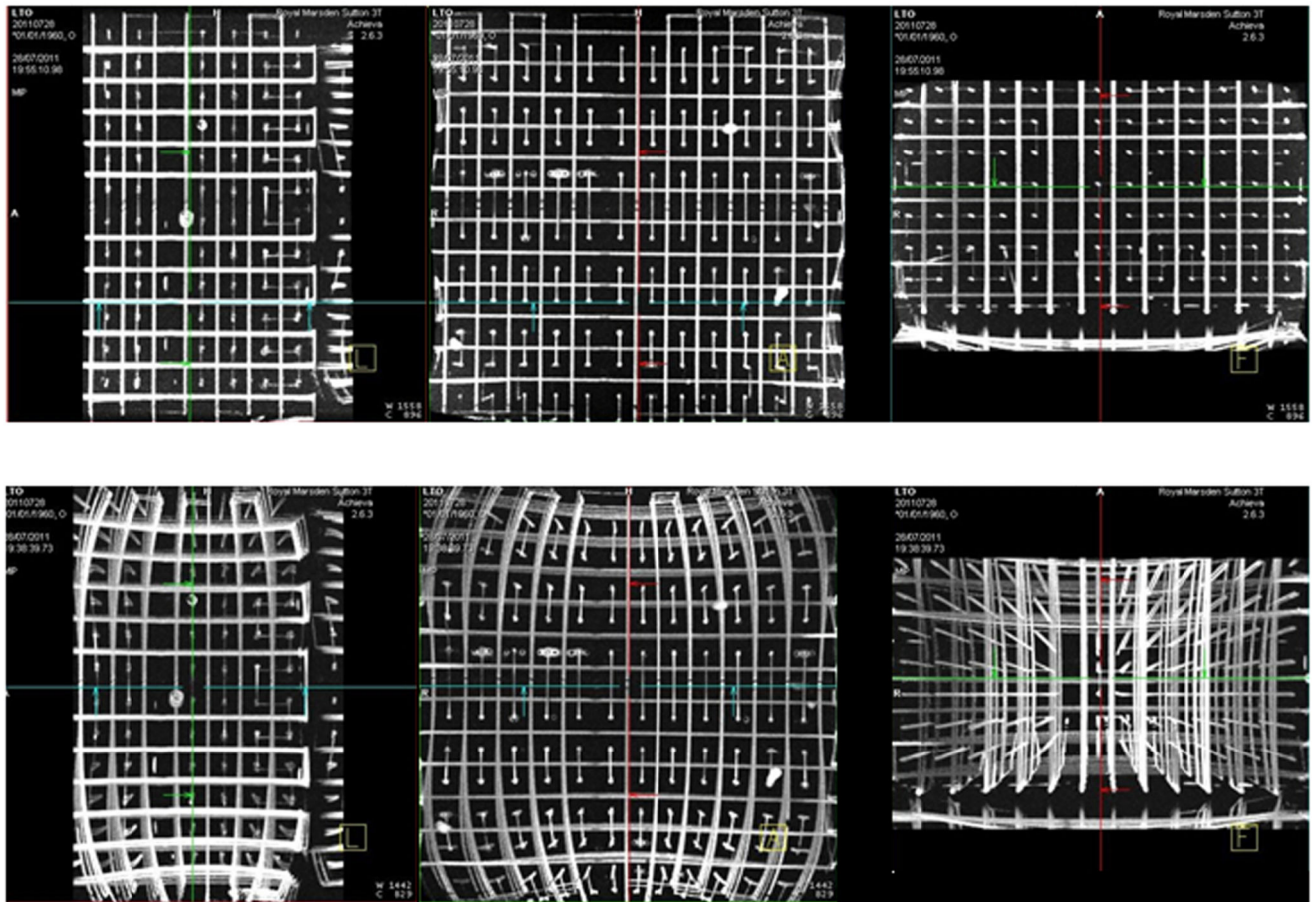


Figure 7. Sagittal, Coronal and Transaxial Maximum Intensity Projections (MIPs) of images of the Linear Test Object described by Doran et al. (2005). The 3D datasets were acquired at 1.5T (Siemens Aera, Erlangen, Germany), using T_1 -weighted sequences normally used for RT planning. The maximum intensity projections (MPSs) on the bottom row show substantial distortions. The MIPS on top row were obtained after applying the built-in distortion correction software provided by the MRI manufacturer.

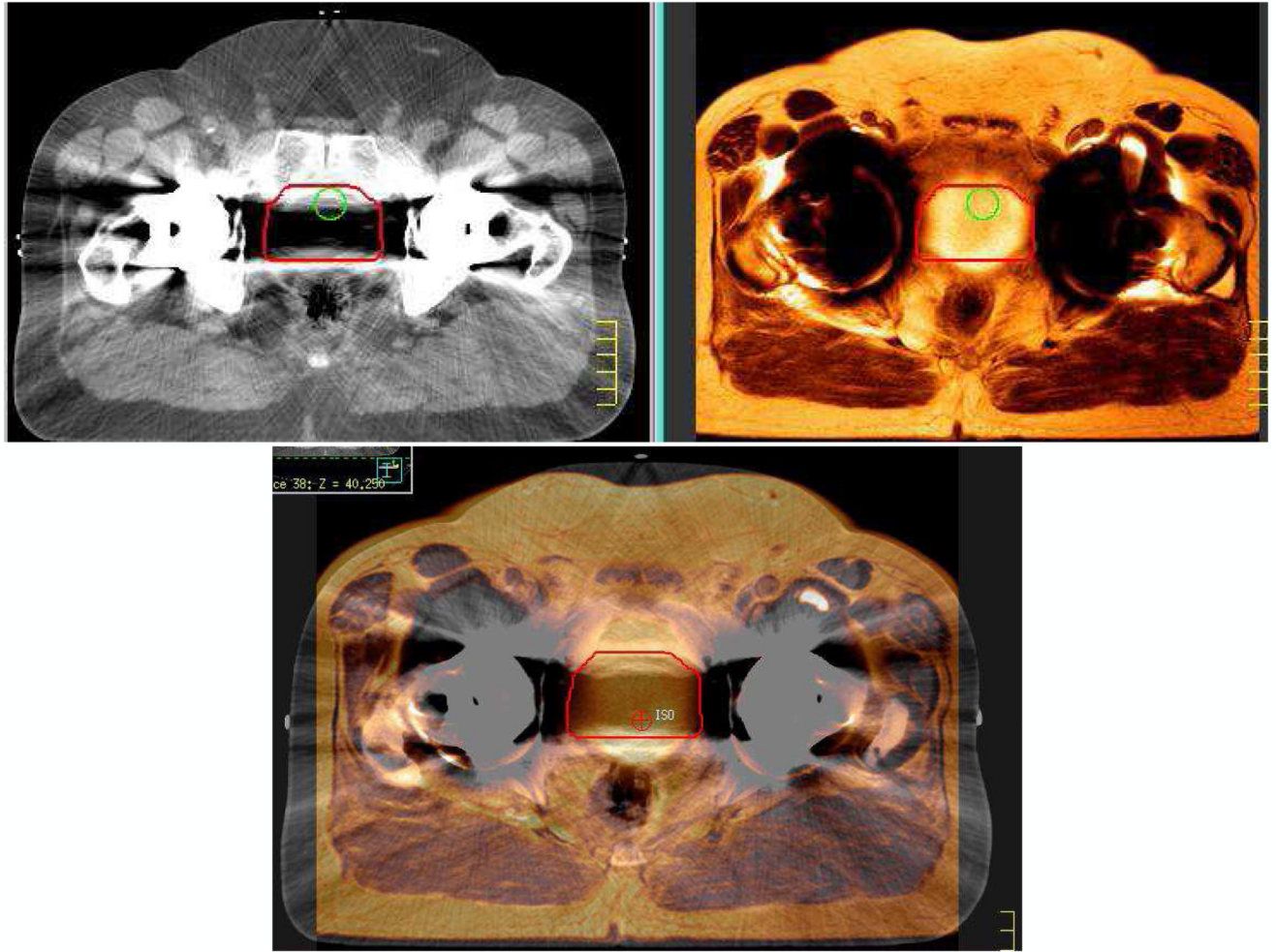


Figure 8.

RT planning images of prostate bed (red outline) in subject with double hip replacement (Pinnacle Planning System, Philips, Best, Netherlands). CT image (top left) is degraded by streak artifacts which prevent demonstration of the prostate bed. MR image (top right) is degraded by signal loss in the vicinity of the metallic implants. In combination, the fused dataset (bottom row) allows successful RT planning, but successful registration is based on structures located away from the implant.

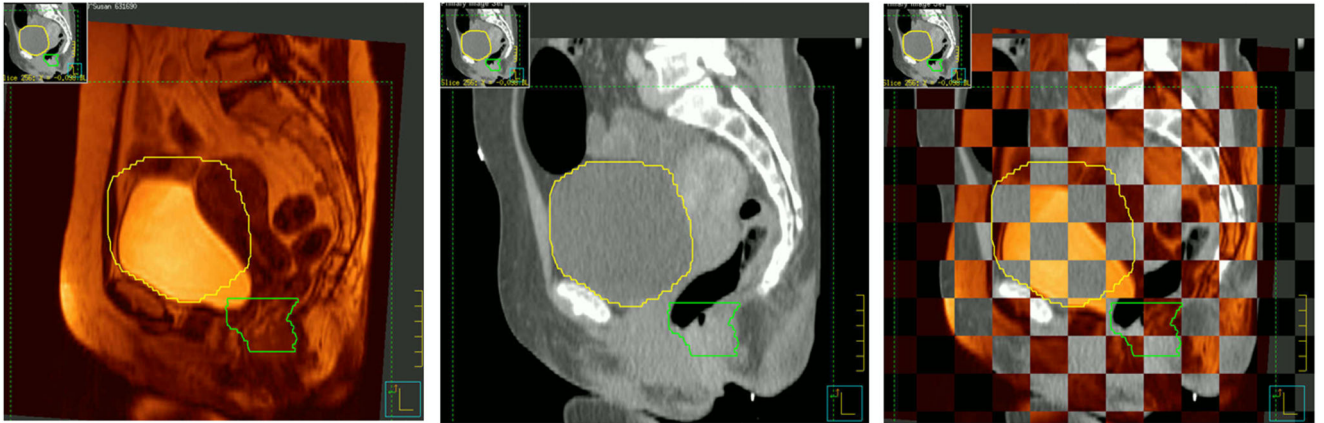


Figure 9.

CT-MR fusion of rectal cancer patient. Both examinations were undertaken using a flat bed and the position of pelvic bones coincides almost perfectly. However, bladder filling is quite different and many soft tissues, including the rectum, are considerably displaced. The benefit of MRI for this particular RT treatment plan is thus limited.

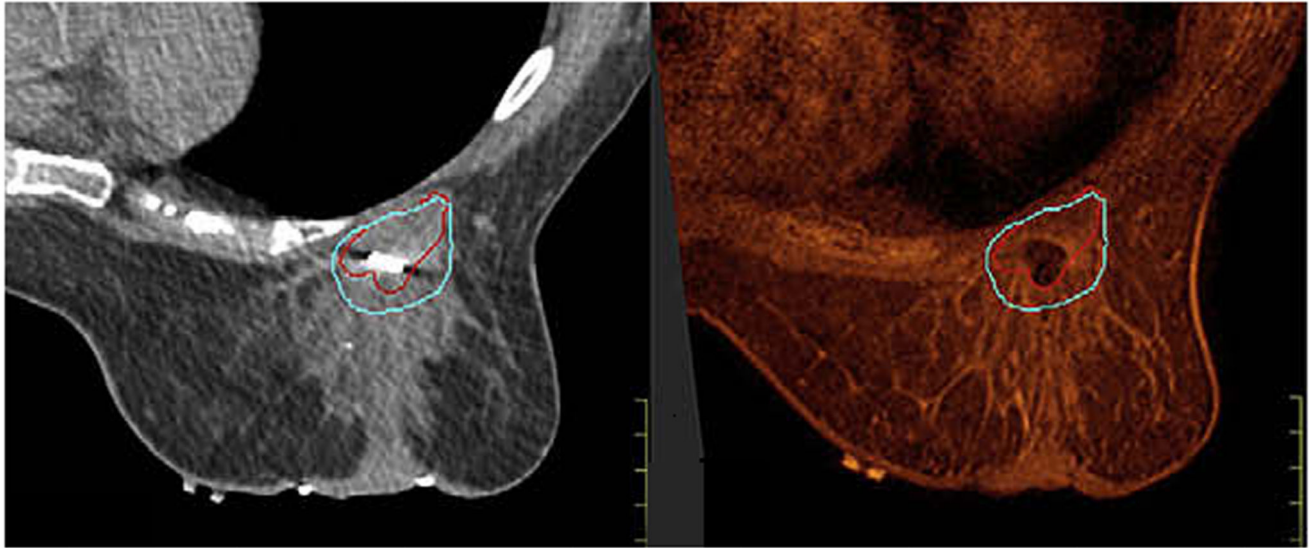


Figure 10.

RT planning study with prone breast examination with multi-modality skin marker (arrow), visible in CT (left) and MR (right). Surgical clips in the tumour bed appear dark in MR images and are surrounded by signal loss.

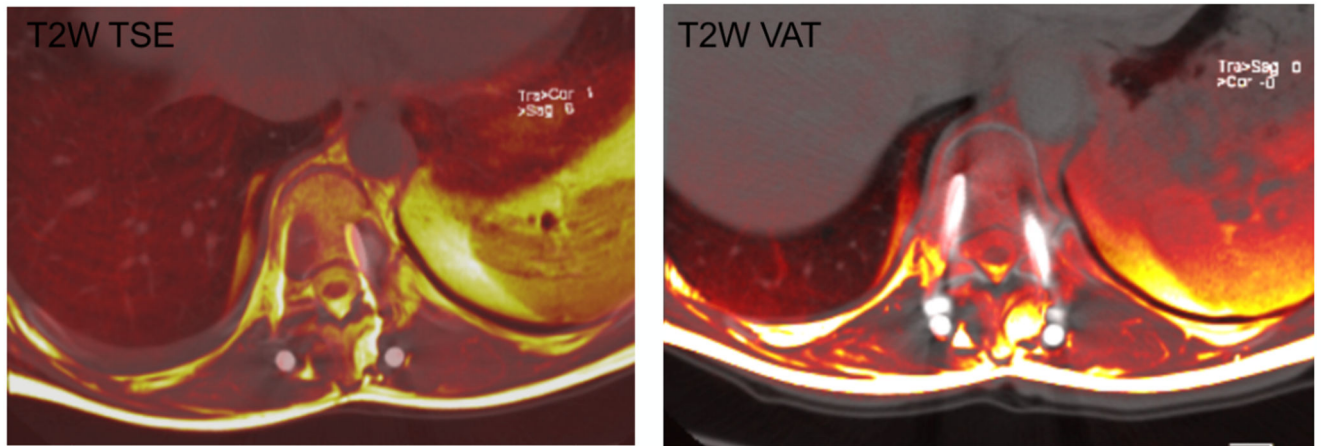


Figure 11. MR-CT fusion on patient with metallic fixation device for spinal stabilisation. The standard T2-weighted MR images (left) show a larger asymmetric area of signal loss surrounding the implant. The signal loss is reduced by employing specialist metal artifact reduction techniques (right).

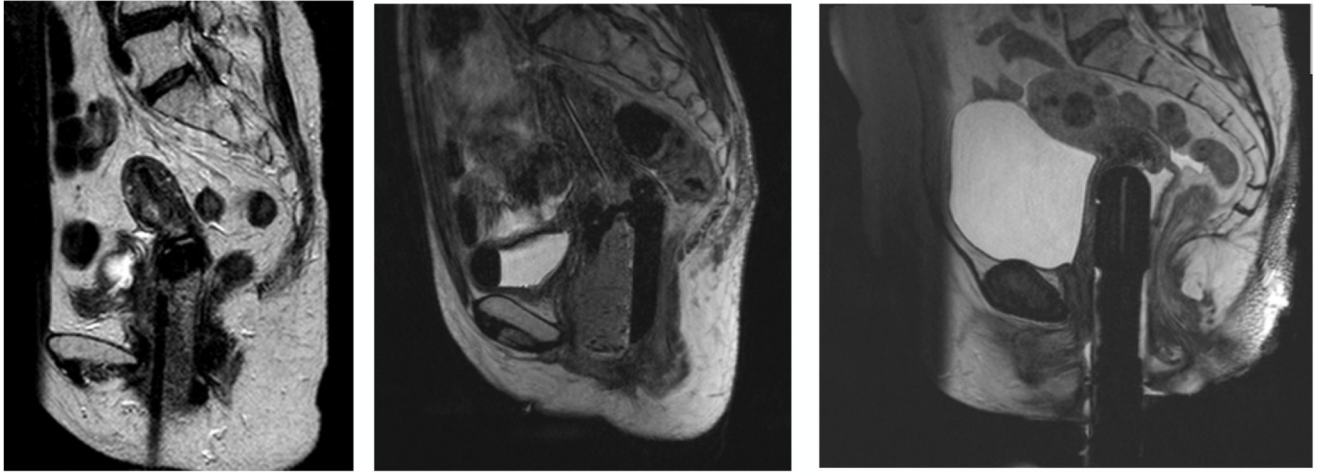


Figure 12.

T₂-weighted MR images of three different types of MR compatible brachytherapy applicators, which appear dark in contrast with surrounding tissue. In the central figure, a fluid filled tube appears bright within applicator. In some cases an anterior saturation band is employed to eliminate signals from the abdominal wall, to prevent motion artifacts in the MR images.

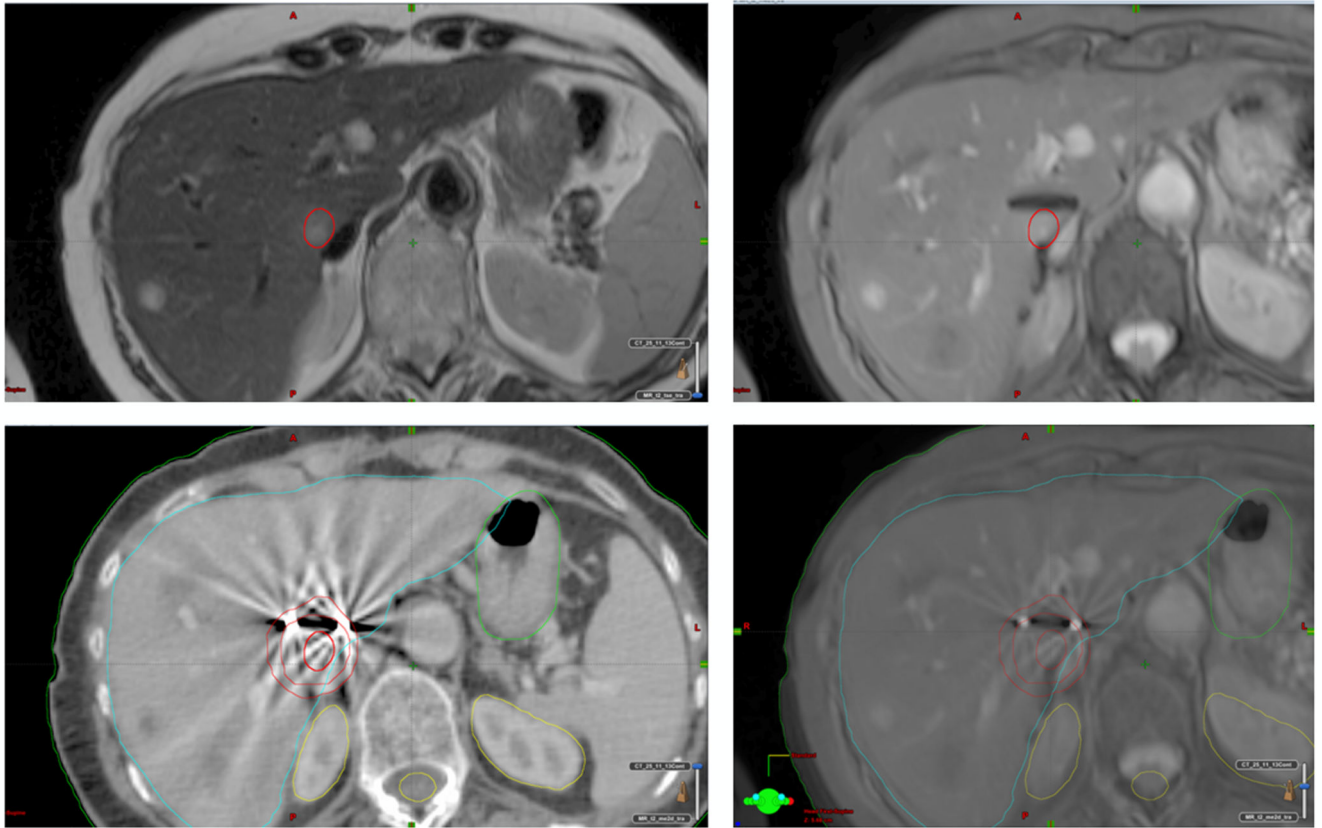


Figure 13.

T2-weighted (top left) and T2*-weighted (top right) MR liver images after insertion of markers for cyberknife stereotatic RT. T2W images allow delineation of the lesion (in red) but do not demonstrate the markers. T2*W images and the CT images (bottom left) allow visualisation of the markers, and therefore can be registered. The CTV is thus transferred to the CT images for RT planning. The combined final dataset (bottom right, created using Eclipse, Varian Medical Systems, Switzerland) shows the CTV outlined using the MRI dataset and the OARs outlined in the CT dataset.